

Joint beamforming and mode optimization for multi-functional STAR-RIS-aided integrated sensing and communication networks

Ziming Liu, *Member, IEEE*, Tao Chen, *Member, IEEE*, Giacinto Gelli, *Senior Member, IEEE*, Vincenzo Galdi, *Fellow, IEEE*, and Francesco Verde, *Senior Member, IEEE*

Abstract—This paper investigates the design of integrated sensing and communication (ISAC) systems assisted by simultaneously transmitting and reflecting reconfigurable intelligent surfaces (STAR-RISs), which act as multi-functional programmable metasurfaces capable of supporting concurrent communication and sensing within a unified architecture. We propose a two-stage ISAC protocol, in which the preparation phase performs direction estimation for outdoor users located in the reflection space, while maintaining communication with both outdoor and indoor users in the transmission space. The subsequent communication phase exploits the estimated directions to enhance information transfer. The directions of outdoor users are modeled as Gaussian random variables to capture estimation uncertainty, and the corresponding average communication performance is incorporated into the design. Building on this framework, we formulate a performance-balanced optimization problem that maximizes the communication sum-rate while guaranteeing the required sensing accuracy, jointly determining the beamforming vectors at the base station (BS), the STAR-RIS transmission and reflection coefficients, and the metasurface partition between energy-splitting and transmit-only modes. The physical constraints of STAR-RIS elements and the required sensing performance are explicitly enforced. To address the non-convex nature of the problem, we combine fractional programming, Lagrangian dual reformulation, and successive convex approximation. The binary metasurface partition is ultimately recovered via continuous relaxation followed by projection-based binarization. Numerical results demonstrate that the proposed design achieves an effective trade-off between sensing accuracy and communication throughput, by significantly outperforming conventional STAR-RIS-aided ISAC schemes. Such characteristics make the proposed architecture well suited for dense Internet-of-Things deployments in smart environments, where energy-efficient connectivity and device localization must be jointly supported.

Index Terms—Beamforming optimization, direction-of-arrival (DOA) estimation, fractional programming, integrated sensing and communication (ISAC), multi-functional programmable metasurfaces, simultaneously transmitting and reflecting (STAR) metasurface, sixth-generation (6G) networks, successive convex

Manuscript received February 18, 2026; revised xx yy, 2026; accepted xx yy, 2026. The associate editor coordinating the review of this paper and approving it for publication was Dr. xx yy. (*Corresponding author: Francesco Verde*)

Z. Liu and T. Chen are with the College of Information and Communication Engineering of Harbin Engineering University, Harbin, 150001 China (e-mail: lzmfred@hrbeu.edu.cn, chentao@hrbeu.edu.cn). G. Gelli is with the Department of Electrical Engineering and Information Technology, University Federico II, Naples I-80125, Italy (e-mail: gelli@unina.it). V. Galdi is with the Department of Engineering, University of Sannio, Benevento I-82100, Italy (e-mail: vgaldi@unisannio.it). F. Verde is with the Department of Engineering, University of Campania Luigi Vanvitelli, Aversa I-81031, Italy (e-mail: francesco.verde@unicampania.it).

approximation (SCA).

I. INTRODUCTION

METASURFACES are artificial electromagnetic (EM) structures composed of subwavelength elements (“meta-atoms”) possibly integrated with tunable microelectronic components, such as diodes and varactors, which enable programmable control over the amplitude, phase, and polarization of incident waves [1]. When empowered with reconfigurability, these structures give rise to *reconfigurable intelligent surfaces (RISs)*, which have emerged as a key enabler for next-generation wireless networks due to their ability to reshape the propagation environment in a software-defined manner [2]–[4]. By dynamically manipulating the reflected or transmitted wavefronts, RISs allow the establishment of favorable communication links, mitigation of blockages, and enhancement of coverage in complex propagation scenarios [5]–[7]. Owing to their low power consumption, compact form factor, and deployment flexibility, RISs are particularly attractive for integration into urban infrastructures, vehicles, and buildings, thus supporting the vision of environment-aware and user-centric wireless networks [8]–[11].

Despite their advantages, conventional RIS architectures typically rely on reflective elements, which inherently limit their angular coverage to a single half-space. This constraint restricts their applicability in scenarios where users are distributed on both sides of the surface. To overcome this limitation, *simultaneously transmitting and reflecting reconfigurable intelligent surfaces (STAR-RISs)* have been recently proposed [12]–[14]. By leveraging advanced meta-atom designs and interlayer structures, STAR-RISs are capable of concurrently reflecting and transmitting incident signals, thereby enabling full-space EM control [15], [16]. This unique capability makes STAR-RISs a promising solution for supporting heterogeneous users located in distinct spatial regions, such as indoor and outdoor environments separated by a building facade.

STAR-RISs can operate under different working *modes*, including energy splitting (ES), mode switching (MS), time division (TD), polarization division (PD), and frequency division (FD) [17], [18]. Among these, the ES mode has received the most attention in the literature due to its ability to simultaneously support transmission and reflection while respecting energy conservation principles [19]–[25]. In this

mode, the transmitted and reflected signals are intrinsically coupled through both amplitude and phase constraints. Other modes, such as MS and TD [26], can be interpreted as special cases or extensions of the ES mode with additional constraints, while PD and FD impose stringent requirements on signal polarization or frequency selectivity [27], [28], and have therefore received limited attention in the literature.

In parallel with the development of programmable metasurfaces, *integrated sensing and communication (ISAC)* has emerged as a fundamental paradigm for sixth-generation (6G) wireless networks [29], [30]. ISAC aims to unify sensing and communication functionalities within a single system, enabling spectrum- and hardware-efficient operation. STAR-RISs are particularly well suited for ISAC applications, as their full-space control capability allows simultaneous information delivery and environmental sensing in different spatial regions. Recent works have investigated STAR-RIS-assisted ISAC systems under various assumptions [31]–[34]. However, most existing designs rely on idealized knowledge of user locations or directions and do not explicitly account for the intrinsic uncertainty arising from sensing and estimation processes. Indeed, in practical ISAC deployments, especially in dynamic outdoor environments, user positions or directions are not perfectly known and must be inferred through sensing mechanisms. Prior studies [35]–[38] have shown that direction-of-arrival (DOA) estimation accuracy in metasurface-assisted systems is fundamentally limited by noise, propagation conditions, and hardware constraints. Moreover, most existing works focus on optimizing beamforming and STAR-RIS coefficients within a single transmission stage. In contrast, the protocol-level design (i.e., the joint optimization of system parameters across multiple phases within a slot) accounting for the distinct roles of sensing- and communication-oriented signaling has received comparatively limited attention.

A. Contribution

This paper investigates a STAR-RIS-aided ISAC system deployed on the façade of a smart building (see Fig. 1), where a base station (BS) serves both indoor and outdoor users while sensing the directions of outdoor users through dedicated sensors mounted on the STAR-RIS. Beyond conventional broadband services, the proposed STAR-RIS-assisted ISAC framework is particularly well suited to support Internet-of-Things (IoT) ecosystems in smart cities [39]. Its low-power, compact metasurface deployment on building facades enables wide-area, environment-aware connectivity and accurate device localization - supporting IoT use cases such as large-scale sensor networks, crowd and traffic monitoring, asset tracking, and energy-efficient massive access in dense urban scenarios.

We propose a two-stage ISAC protocol operating on a slot-by-slot basis. In the preparation phase, the system performs DOA estimation for outdoor users while simultaneously supporting downlink communication to all users. In the subsequent communication phase, the estimated angular information is exploited to refine the transmission strategy and enhance sum-rate communication performance. In order to explicitly capture the effect of sensing uncertainty, the directions of

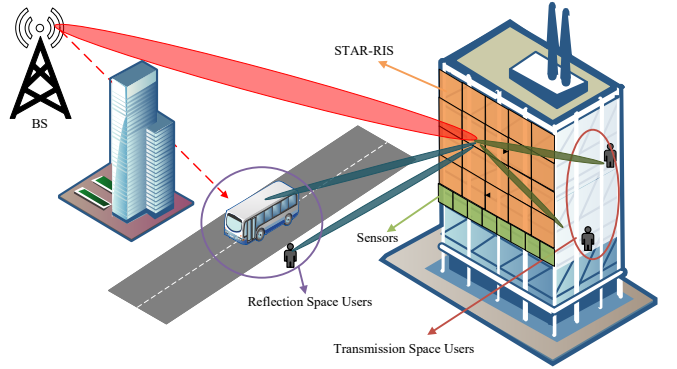


Figure 1: Illustration of the considered STAR-RIS-aided network.

outdoor users are modeled as Gaussian random variables whose variances are determined by estimation accuracy, and the average communication and sensing performance is incorporated into the system design.

Building on this framework, we formulate a performance-balanced optimization problem that jointly designs the base station beamforming vectors, the STAR-RIS transmission and reflection coefficients in both stages, and the metasurface partition between ES and transmit-only (TO) modes, where each element fully transmits the incident signal without power splitting. The physical feasibility constraints of STAR-RIS elements, including energy conservation and phase coupling, are explicitly enforced, together with sensing-quality requirements. To tackle the resulting non-convex and mixed discrete-continuous optimization problem, we derive an efficient solution based on fractional programming, Lagrangian dual reformulation, successive convex approximation, and semidefinite relaxation. The binary metasurface partition is ultimately recovered through a continuous relaxation followed by projection-based binarization. Simulation results demonstrate that the proposed design achieves a favorable trade-off between sensing accuracy and communication throughput, while exhibiting robustness against direction estimation errors. Compared with conventional STAR-RIS-aided ISAC schemes that neglect uncertainty or multi-functional operation, the proposed framework yields significant performance gains under both ideal and imperfect sensing conditions.

B. Organization

The remainder of the paper is organized as follows. Section II presents the system model and the basic assumptions considered throughout the paper, including the STAR-RIS architecture, the two-stage ISAC protocol, and the DOA uncertainty model for outdoor users. Section III formulates the optimization problem and derives the proposed algorithmic solution. Section IV provides numerical results and performance comparisons. Section V concludes the paper.

II. SYSTEM MODEL AND BASIC ASSUMPTIONS

As shown in Fig. 1, we consider an ISAC system, where sensing and communication tasks are assisted by a STAR-RIS,

placed on the outer wall of a smart building, which is a realistic deployment strategy in future smart cities and 6G intelligent environments [40]. Smart buildings already integrate multiple technologies (e.g., heating, ventilation, air conditioning, lighting, and surveillance). In accordance with the emerging paradigm of user-centric and environment-aware networks, we envision a smart building additionally incorporating radio-frequency (RF) sensors aimed at detecting and localizing low-mobility users in the vicinity of the facade [39]. Sensors on the wall have direct visibility toward the front zone of the building, making them ideal for real-time, accurate localization, which is a crucial issue in many applications of environmental sensing, such as, e.g., crowd monitoring, pedestrian flow analysis, public transportation systems monitoring [41], and traffic control.

The considered ISAC system consists of a BS, equipped with a uniform linear array (ULA) of M antennas, which transmits in downlink to K users. The STAR-RIS is composed by a uniform planar array (UPA) of $N = N_x \times N_z$ reconfigurable elements, which enable full-space control. The impinging EM signals can be reflected from the STAR-RIS for outdoor sensing and communication, and can be simultaneously transmitted (i.e., refracted) for indoor information transfer.

We assume that K_R single-antenna users reside in the outdoor reflection side (*reflection space*) and K_T single-antenna users lie in the indoor transmission side (*transmission space*). Hereinafter, for the sake of conciseness, the set $\mathcal{K} \triangleq \{1, 2, \dots, K\}$, with $K \triangleq K_T + K_R$, collects the indexes of both indoor and outdoor receivers: the first K_T entries of \mathcal{K} (belonging to the set $\mathcal{K}_T \triangleq \{1, 2, \dots, K_T\}$) identify the indoor terminals, whereas the remaining K_R ones (belonging to the set $\mathcal{K}_R \triangleq \{K_T + 1, K_T + 2, \dots, K\}$) are used to index the outdoor ones. Similarly to [31], we consider a sensing-at-STAR-RIS structure, where a dedicated low-cost sensor with a ULA consisting of N_s elements is mounted on the STAR-RIS.

The direct BS-to-user links are assumed negligible (in number) compared to the STAR-RIS-assisted paths, due to severe blockage and unfavorable propagation conditions, typical of indoor and outdoor urban environments. Such an assumption is supported by standardized models and field measurements at mmWave or sub-THz frequencies, which show that building penetration loss and blockage effects may render indoor paths negligible. For example, 3GPP TR 38.901 [42] and ITU-R P.2109 [43] report penetration losses often exceeding 30–60 dB for common construction materials, while extensive urban measurements (e.g., NYU Wireless [44]) confirm that severe strong attenuation (e.g., by buildings or foliage) is not rare in dense urban outdoor deployments.

The observation interval is divided into time slots of duration T over which the channels and direction parameters of the users are assumed to be constant. All the relevant channels are modeled as frequency-flat (i.e., the channel delay spread is small relative to the inverse signal bandwidth), as detailed in Subsection II-C. During the t -th slot, with $t \in \mathbb{N}_0$, the direction of the k -th user is described by $\mathbf{d}_k(t) \triangleq [\phi_k(t), \varphi_k(t)]^T \in \mathbf{R}^2$, where $\phi_k(t)$ and $\varphi_k(t)$ are the elevation and azimuth angles between the k -th user and the STAR-RIS, respectively, for $k \in \mathcal{K}$. We assume perfectly known directions for indoor users [45], i.e., $\mathbf{d}_1(t), \mathbf{d}_2(t), \dots, \mathbf{d}_{K_T}(t)$ are treated as known

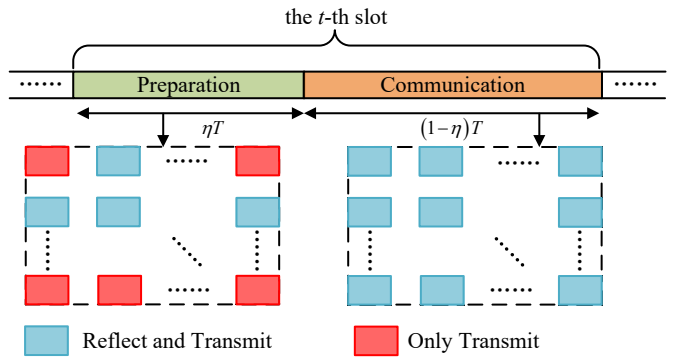


Figure 2: Working modes of the STAR-RIS in a generic slot.

deterministic parameters in the optimization process. Such an assumption is justified by the fact that indoor users are typically connected via fixed access points with well-defined geometric layouts and, thus, their positions and orientations can be precisely estimated through existing localization and tracking systems. Moreover, since the indoor propagation environment is quasi-static, the directions of indoor users are often stable over long time intervals. Conversely, the directions of outdoor users cannot be assumed as perfectly known, since outdoor environments are typically dynamic and unpredictable, making directions of outdoor users observable only through estimation mechanisms working on a slot-by-slot basis [46].

As shown in Fig. 2, the time slot t is divided into two subslots. The first one, of duration ηT (with $0 \leq \eta \leq 1$ being a fixed system parameter) is referred to as the *preparation phase* or *stage*, and is dedicated to sensing of the outdoor users, i.e., estimation of the directions $\mathbf{d}_{K_T+1}(t), \mathbf{d}_{K_T+2}(t), \dots, \mathbf{d}_K(t)$, and downlink communication to both indoor and outdoor users. During such a phase, reflection signals towards the outdoor users are realized by the STAR-RIS relying on the estimates of the outdoor user directions obtained in the previous $(t-1)$ -th slot (see Subsections II-C and II-E). Capitalizing on the estimates $\hat{\mathbf{d}}_{K_T+1}(t), \hat{\mathbf{d}}_{K_T+2}(t), \dots, \hat{\mathbf{d}}_K(t)$ of the outdoor user directions obtained at the end of the preparation stage during the t -th slot, the remaining part of the slot of duration $(1 - \eta) T$, referred to as *communication phase/stage*, is only devoted to information transfer to all the users.

As the ISAC system operates on a slot-by-slot basis, the analysis is restricted, without loss of generality, to a generic time slot. Accordingly, in the following the explicit dependence on the slot index t is omitted, unless otherwise indicated.

A. Signal transmitted by the BS

We assume that sensing of the outdoor devices is performed using the same signals employed for communication. This design choice is primarily motivated by the need to enhance spectral and hardware efficiencies, thereby minimizing bandwidth consumption, reducing system complexity, and lowering implementation costs. During a given time slot, the signal transmitted by the BS to the k -th user in the i -th symbol interval

can be written as

$$\mathbf{x}(i) = \mathbf{W} \mathbf{s}(i) = \sum_{k=1}^K \mathbf{w}_k s_k(i),$$

for $i \in \mathcal{I} \triangleq \{0, 1, \dots, I-1\}$ (1)

where I is the number of symbols packed by the BS in a slot, $\mathbf{W} = [\mathbf{w}_1, \mathbf{w}_2, \dots, \mathbf{w}_K] \in \mathbb{C}^{M \times K}$ represents the beamforming matrix and $\mathbf{s}(i) = [s_1(i), s_2(i), \dots, s_K(i)]^T \in \mathbb{C}^K$ denotes the signal vector, with $s_k(i)$ ($k \in \mathcal{K}$) denoting the signal destined to the k -th user. In the sequel, we assume that $\mathbf{s}(i)$ can be modeled as a zero-mean complex circular vector having covariance matrix $\mathbb{E}[\mathbf{s}(i) \mathbf{s}^H(i)] = \mathbf{I}_K$, which is statistically independent of the information-bearing symbols transmitted in other symbol intervals and slots. This signal model remains valid across all operational modes of the system. Using (1), the total power transmitted by the BS is

$$\mathcal{P} \triangleq \mathbb{E}[\|\mathbf{x}(i)\|^2] = \text{tr}(\mathbf{W} \mathbf{W}^H). \quad (2)$$

B. STAR-RIS model

We assume that the STAR-RIS is located in the far-field region of the BS and, additionally, all the users are in the far-field region of the STAR-RIS. Moreover, we make the customary assumption that the one-sided bandwidth B of the ISAC signal is much smaller than its carrier frequency f_0 , thereby ensuring that the responses of the BS array and RIS are essentially constant within the frequency interval $(f_0 - \frac{B}{2}, f_0 + \frac{B}{2})$. Finally, we consider a linearly polarized (horizontally or vertically) wireless signal, and we neglect cross-polarization effects and losses. The RIS elements, which are arranged in a rectangular grid, are indexed row by row. If they are designed such that to ensure weak dependence on the incidence direction [47], the EM response of its n -th element during the preparation stage is described by the transmission coefficient

$$\phi_{T,n}^p = \beta_{T,n}^p e^{j\theta_{T,n}^p} \quad (3)$$

where $j \triangleq \sqrt{-1}$ denotes the imaginary unit, controlling the transmitted fraction of the incident wave, and the reflection coefficient

$$\phi_{R,n}^p = \beta_{R,n}^p e^{j\theta_{R,n}^p} \quad (4)$$

dictating the reflected fraction of the incident wave, where $\beta_{a,n}^p$ and $\theta_{a,n}^p$ represent the amplitude and phase of the n -th element during the preparation stage, respectively, for $a \in \{T, R\}$ and $n \in \mathcal{N} \triangleq \{1, 2, \dots, N\}$. The coupling between the reflection and transmission coefficients of each element depends on the operational mode of the STAR-RIS.

During the preparation stage, each element of the STAR-RIS might independently work either in ES or TO modes [17]. In the case of ES, the signal transmitted by the n -th element of the BS is simultaneously reflected outdoor and transmitted indoor in the preparation stage. Two constraints have to be fulfilled for passive lossless STAR-RIS in ES mode. First, according to the law of energy conservation [48], the incident signal's power on the element must be equal to the sum of reflected and transmitted powers. Second, since the

scalar electric and magnetic impedances of the n -th element of the STAR-RIS should have purely imaginary values, the phases of the reflection and transmission coefficients obey $\cos(\theta_{R,n}^p - \theta_{T,n}^p) = 0$ [20]. To be more specific, the two constraints in ES mode can be stated as follows

$$(\beta_{R,n}^p)^2 + (\beta_{T,n}^p)^2 = 1 \quad (5)$$

$$\theta_{R,n}^p - \theta_{T,n}^p = \frac{\pi}{2} \text{ or } \frac{3\pi}{2}. \quad (6)$$

Alternatively, for the TO configuration, the n -th element of the STAR-RIS operates during the preparation stage in transmission mode solely, i.e.,

$$\beta_{R,n}^p = 0 \quad \text{and} \quad \beta_{T,n}^p = 1 \quad (7)$$

$$\theta_{T,n}^p \in [-\pi, \pi]. \quad (8)$$

Therefore, transmission and reflection coefficients are straightforwardly decoupled in this case. To formally characterize the aforementioned two operating configurations during the preparation stage in a compact manner, we introduce a binary selection vector $\mathbf{b} \triangleq [b_1, b_2, \dots, b_N]^T \in \{0, 1\}^N$, where each entry $b_n \in \{0, 1\}$ indicates the working mode of the n -th element of the STAR-RIS. Specifically, when $b_n = 1$, the n -th element operates in ES mode and, thus, the transmission and reflection coefficients (3) and (4) obey the constraints (5) and (6). Otherwise, $\phi_{T,n}^p$ and $\phi_{R,n}^p$ fulfill the constraints (7) and (8) if $b_n = 0$ and, hence, the n -th element works in TO manner. By constraining the L^1 -norm of the vector \mathbf{b} to assume a specific value $N_{\text{part}} \leq N$, one may enforce a *dynamic partition* of the STAR-RIS during the preparation phase, according to which N_{part} out of its N elements work in ES mode, while the remaining $N - N_{\text{part}}$ ones are TO elements. Such a partition allows the system to flexibly balance communication throughput and sensing accuracy in the preparation phase.

In the communication stage, *all* the elements of the STAR-RIS are optimized to maximize communication performance for both indoor and outdoor users, i.e.,

$$(\beta_{R,n}^c)^2 + (\beta_{T,n}^c)^2 = 1 \quad (9)$$

$$\theta_{R,n}^c - \theta_{T,n}^c = \frac{\pi}{2} \text{ or } \frac{3\pi}{2} \quad (10)$$

$\forall n \in \{1, 2, \dots, N\}$, where $\beta_{a,n}^c$ and $\theta_{a,n}^c$ represent the amplitude and phase of the n -th element of the STAR-RIS during the communication stage, respectively, for $a \in \{T, R\}$.

For $a \in \{p, c\}$, the STAR-RIS is collectively described by the diagonal matrices $\Phi_R^a \in \mathbb{C}^{N \times N}$ and $\Phi_T^a \in \mathbb{C}^{N \times N}$, gathering the reflection and transmission coefficients of the STAR-RIS, respectively, which can be expressed as

$$\Phi_R^p \triangleq \mathbf{B} \text{diag} \left(\tilde{\beta}_{R,1}^p e^{j\theta_{R,1}^p}, \tilde{\beta}_{R,2}^p e^{j\theta_{R,2}^p}, \dots, \tilde{\beta}_{R,N}^p e^{j\theta_{R,N}^p} \right) \quad (11)$$

$$\Phi_T^p \triangleq \text{diag} \left(\beta_{T,1}^p e^{j\theta_{T,1}^p}, \beta_{T,2}^p e^{j\theta_{T,2}^p}, \dots, \beta_{T,N}^p e^{j\theta_{T,N}^p} \right) \quad (12)$$

$$\Phi_a^c \triangleq \text{diag} \left(\beta_{a,1}^c e^{j\theta_{a,1}^c}, \beta_{a,2}^c e^{j\theta_{a,2}^c}, \dots, \beta_{a,N}^c e^{j\theta_{a,N}^c} \right) \quad (13)$$

with $\mathbf{B} \triangleq \text{diag}(b_1, b_2, \dots, b_N)$ and $a \in \{T, R\}$. In this framework, the reflection amplitude of the n -th element of the STAR-RIS during the preparation stage turns out to be $\beta_{R,n}^p = b_n \tilde{\beta}_{R,n}^p$, for $n \in \mathcal{N}$. It is worthwhile to note that our optimization framework involve not only the physical

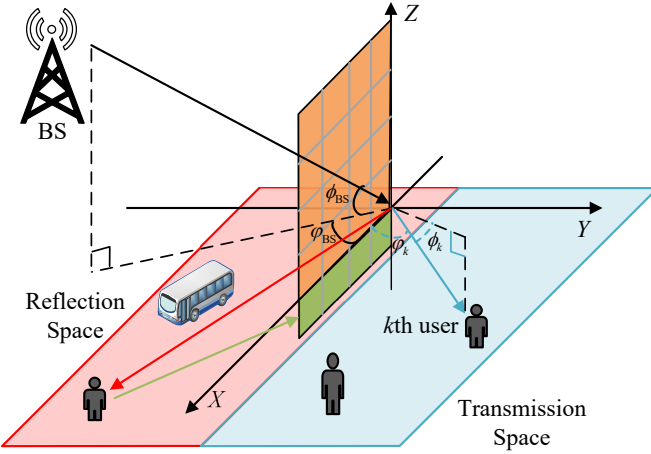


Figure 3: Angular representation of the ISAC system model.

parameters of the STAR-RIS (i.e., amplitude and phases) but also the mode-selection vector \mathbf{b} in the preparation stage.

C. Channel model

For all wireless links, we employ a quasi-static frequency-flat Rician fading channel model [13]. Specifically, denoting with $\mathbf{H}_1 \in \mathbb{C}^{N \times M}$ the channel from the BS to the STAR-RIS and with $\mathbf{H}_2 \triangleq [\mathbf{H}_{2,\text{in}}^T, \mathbf{H}_{2,\text{out}}^T]^T \in \mathbb{C}^{K \times N}$ the channel from the STAR-RIS to the K users, with $\mathbf{H}_{2,\text{in}} \in \mathbb{C}^{K_{\text{R}} \times N}$ and $\mathbf{H}_{2,\text{out}} \in \mathbb{C}^{K_{\text{R}} \times N}$, the composite channels can be expressed as

$$\mathbf{H}_1 = \sqrt{\frac{1}{\varsigma_1}} \left(\sqrt{\frac{\mu_1}{1 + \mu_1}} \mathbf{H}_1^{\text{LoS}} + \sqrt{\frac{1}{1 + \mu_1}} \mathbf{H}_1^{\text{NLoS}} \right) \quad (14)$$

$$\mathbf{H}_{2,\text{in}} = \mathbf{P}_{\text{in}}^{-1/2} \left(\sqrt{\frac{\mu_{2,\text{in}}}{1 + \mu_{2,\text{in}}}} \mathbf{H}_{2,\text{in}}^{\text{LoS}} + \sqrt{\frac{1}{1 + \mu_{2,\text{in}}}} \mathbf{H}_{2,\text{in}}^{\text{NLoS}} \right) \quad (15)$$

$$\mathbf{H}_{2,\text{out}} = \mathbf{P}_{\text{out}}^{-1/2} \left(\sqrt{\frac{\mu_{2,\text{out}}}{1 + \mu_{2,\text{out}}}} \mathbf{H}_{2,\text{out}}^{\text{LoS}} + \sqrt{\frac{1}{1 + \mu_{2,\text{out}}}} \mathbf{H}_{2,\text{out}}^{\text{NLoS}} \right) \quad (16)$$

where ς_1 is the path loss of the BS-to-STAR-RIS channel, whereas $\mathbf{P}_{\text{in}} \triangleq \text{diag}(\varsigma_{\text{in},1}, \varsigma_{\text{in},2}, \dots, \varsigma_{\text{in},K_{\text{R}}})$ collects the path losses of the channels between the STAR-RIS and the indoor users, $\mathbf{P}_{\text{out}} \triangleq \text{diag}(\varsigma_{\text{out},1}, \varsigma_{\text{out},2}, \dots, \varsigma_{\text{out},K_{\text{R}}})$ gathers the path losses of the channels between the STAR-RIS and the outdoor users. For the generic ℓ -th link, we adopt as path-loss model $\varsigma_\ell = \varsigma_0 (d_\ell/d_0)^{-\kappa_\ell}$, with d_ℓ denoting the propagation distance, d_0 being the reference distance (typically 1 m), ς_0 representing the reference path loss at d_0 , and κ_ℓ indicating the path loss exponent. Moreover, in (14), (15), and (16) $\mu_1, \mu_{2,\text{in}}, \mu_{2,\text{out}} > 0$ are the Rice factors of the corresponding channels, whereas $\{\mathbf{H}_{2,\text{in}}^{\text{LoS}}, \mathbf{H}_{2,\text{out}}^{\text{LoS}}\}$ and $\{\mathbf{H}_{2,\text{in}}^{\text{NLoS}}, \mathbf{H}_{2,\text{out}}^{\text{NLoS}}\}$ denote the (deterministic) line-of-sight (LoS) component and the (random) nonline-of-sight (NLoS) components.

The NLoS channel entries of the matrices $\mathbf{H}_1^{\text{NLoS}}$ and $\mathbf{H}_2^{\text{NLoS}} \triangleq [\{\mathbf{H}_{2,\text{in}}^{\text{NLoS}}\}^T, \{\mathbf{H}_{2,\text{out}}^{\text{NLoS}}\}^T]^T \in \mathbb{C}^{K \times N}$ are mutually independent, modeled as independent identically-distributed (i.i.d.) complex circularly-symmetric zero-mean unit-variance Gaussian random variables. For the LoS components, we

express them using the array steering vectors of the BS and STAR-RIS. Specifically, under the assumption of half-wavelength inter-element spacing, one has (see Fig. 3)

$$\mathbf{a}_{\text{BS}}(\phi, \varphi) \triangleq \left[1, e^{-j\pi \cos \phi \cos \varphi}, \dots, e^{-j\pi(M-1) \cos \phi \cos \varphi} \right]^T \quad (17)$$

and

$$\begin{aligned} \mathbf{a}_{\text{STAR}}(\phi, \varphi) &= \left[1, e^{-j\pi \sin \phi \cos \varphi}, \right. \\ &\quad \left. \dots, e^{-j\pi(N_x-1) \sin \phi \cos \varphi} \right]^T \\ &\quad \otimes \left[1, e^{-j\pi \sin \varphi}, \dots, e^{-j\pi(N_z-1) \sin \varphi} \right]^T \in \mathbb{C}^N \quad (18) \end{aligned}$$

respectively, with ϕ and φ denoting the elevation and azimuth angles. Consequently, it turns out that

$$\mathbf{H}_1^{\text{LoS}} = \mathbf{a}_{\text{STAR}}(\phi_{\text{BS}}, \varphi_{\text{BS}}) \mathbf{a}_{\text{BS}}^H(\phi_{\text{BS}}, \varphi_{\text{BS}}) \quad (19)$$

with ϕ_{BS} and φ_{BS} (see Fig. 3) denoting the elevation and azimuth angles between the BS and the STAR-RIS. Moreover, the k -th row of $\mathbf{H}_2^{\text{LoS}} \triangleq [\{\mathbf{H}_{2,\text{in}}^{\text{LoS}}\}^T, \{\mathbf{H}_{2,\text{out}}^{\text{LoS}}\}^T]^T \in \mathbb{C}^{K \times N}$ is given by $\mathbf{a}_{\text{STAR}}^H(\phi_k, \varphi_k)$, where we recall (see Fig. 3) that ϕ_k and φ_k are the elevation and azimuth angle between the k -th user and the STAR-RIS.

In this work, the channel between the BS and the STAR-RIS (i.e., the matrix \mathbf{H}_1) is assumed to be perfectly known. This assumption is reasonable and widely adopted in the literature on RIS- and STAR-RIS-assisted ISAC systems (see e.g., [31]–[34]) for several practical and theoretical reasons. First, the BS-to-STAR-RIS link is typically quasi-static and highly deterministic, as the STAR-RIS is deployed at a fixed and known location with a stable orientation relative to the BS. This link primarily consists of a LoS or dominant specular component, which can be accurately characterized during installation or calibration using standard site-survey or backhaul measurements. Second, in ISAC systems, the BS transmits known pilot or sensing waveforms, enabling precise self-sounding of the BS-to-STAR-RIS channel prior to or during regular operation. Since the channel matrix \mathbf{H}_1 changes much more slowly than the dynamic STAR-RIS-to-user channels, its estimation overhead is negligible with respect to the overall system timescale.

Regarding the links among the STAR-RIS and the indoor users, the matrix $\mathbf{H}_{2,\text{in}}$ is assumed to be perfectly known due to the assumption stated above that the directions of indoor users are given and the fact that the rich but wide-sense stationary NLoS multipath of indoor users can be reliably estimated and tracked with negligible training overhead relative to the coherence time. On the other hand, as discussed earlier, the angles of outdoor users relative to the STAR-RIS are generally unknown and must be estimated [46]. Therefore, the LoS components of the STAR-RIS-to-outdoor-user channels (i.e., the matrix $\mathbf{H}_{2,\text{out}}^{\text{LoS}}$) inherently depend on imperfect directional information. Conversely, the NLoS components (i.e., the matrix $\mathbf{H}_{2,\text{out}}^{\text{NLoS}}$) are treated as known, as their small-scale variations can be learned through standard pilot-based channel acquisition within each coherence interval and typically remain quasi-static over short durations. This modeling approach reflects practical ISAC operation [49], [50], in which geometric parameters such as

DOAs are inferred through sensing, while small-scale fading is estimated from communication signaling and updated sufficiently often to maintain reliable channel knowledge.

D. Signal received by the k -th user

According to Fig. 2, we assume hereinafter that the number of symbols per slot is divided as $I = I_p + I_c$, where I_p and I_c are the number of symbols included into the preparation and communication phases, respectively. Consequently, it follows that $\eta = I_p T_s / T$, where T_s denotes the symbol interval. Let $\mathbf{h}_{2,k}^H$ denote the k -th row of the matrix \mathbf{H}_2 , during a given time slot, the signal received by the k -th user in the i -th symbol interval can be written as

$$y_{u,k}(i) = \underbrace{\mathbf{h}_{2,k}^H \Phi_k(i) \mathbf{H}_1 \mathbf{w}_k s_k(i)}_{\text{desired signal}} + \underbrace{\sum_{\substack{h=1 \\ h \neq k}}^K \mathbf{h}_{2,k}^H \Phi_k(i) \mathbf{H}_1 \mathbf{w}_h s_h(i) + n_{u,k}(i)}_{\text{inter-user interference}} \quad (20)$$

for $k \in \mathcal{K}$ and $i \in \{0, 1, \dots, I-1\}$, where

$$\Phi_k(i) = \begin{cases} \Phi^p(k), & \text{for } i \in \{0, 1, \dots, I_p-1\} \\ \Phi^c(k), & \text{for } i \in \{I_p, I_p+1, \dots, I-1\} \end{cases} \quad (21)$$

with

$$\Phi^v(k) = \begin{cases} \Phi_T^v, & \text{for } k \in \mathcal{K}_T \\ \Phi_R^v, & \text{for } k \in \mathcal{K}_R \end{cases} \quad (22)$$

for $v \in \{p, c\}$, and $n_{u,k}(i) \sim \mathcal{CN}(0, \sigma_{n_u}^2)$ is additive white Gaussian noise (AWGN) at the k -th user terminal, with $n_{u,k}(i_1)$ statistically independent of $n_{u,k}(i_2)$ for $i_1 \neq i_2$. Thus, the *signal-to-interference-plus-noise ratio* (SINR) of the k -th user can be defined as

$$\gamma_k^v = \frac{\left| \mathbf{h}_{2,k}^H \Phi^v(k) \mathbf{H}_1 \mathbf{w}_k \right|^2}{\sum_{\substack{p=1 \\ p \neq k}}^K \left| \mathbf{h}_{2,k}^H \Phi^v(k) \mathbf{H}_1 \mathbf{w}_p \right|^2 + \sigma_{n_u}^2} \quad (23)$$

for $k \in \mathcal{K}$ and $v \in \{p, c\}$.

Assuming that the BS encodes the information for each user using an i.i.d. Gaussian code, the achievable sum-rate of the system can be expressed as

$$\mathcal{R} = \eta \mathcal{R}^p + (1 - \eta) \mathcal{R}^c \quad (24)$$

with

$$\mathcal{R}^v = \sum_{k=1}^K \log_2 (1 + \gamma_k^v) \quad (25)$$

for $v \in \{p, c\}$ representing the sum-rate in the preparation/communication stage. In what follows, the total sum-rate \mathcal{R} is assumed as the overall communication performance.

E. Signal received by the sensor

For analytical tractability, it is assumed that the sensor mounted on the STAR-RIS can perfectly separate the echo signals corresponding to the different targets (i.e., outdoor users). This is consistent with recent studies on ISAC systems [31], [33], [51], which employ target-specific signaling or structured processing to make multi-target discrimination feasible. In particular, the echo signals can be processed independently if the targets are sufficiently separated in angle, range, or Doppler domain [31], [51], or when orthogonal modulation sequences are employed [33]. Such an assumption is widely adopted in ISAC literature and can be relaxed in future work to incorporate partial or imperfect target separability.

During the preparation phase of a given time slot, under the assumption of perfect echo separation, the received echo signal at the sensor due to the k -th target can be written as

$$\mathbf{y}_{s,k}(i) = \alpha_k \mathbf{a}_S(\phi_k, \varphi_k) \mathbf{a}_{\text{STAR}}^H(\phi_k, \varphi_k) \Phi_R^p \mathbf{H}_1 \mathbf{x}(i) + \mathbf{n}_s(i) \quad (26)$$

for $k \in \mathcal{K}_R$ and $i \in \{0, 1, \dots, I_p-1\}$, where $\alpha_k \in \mathbb{C}$ is the known complex amplitude determined by the round-trip path-loss and the radar cross section (RCS) of the target, whereas

$$\mathbf{a}_S(\phi_k, \varphi_k) = \left[1, e^{-j\pi \cos \phi_k \cos \varphi_k}, \dots, e^{-j\pi(N_s-1) \cos \phi_k \cos \varphi_k} \right]^T \quad (27)$$

represents the steering vector of the sensor with half-wavelength inter-element spacing, and $\mathbf{n}_s(i) \in \mathbb{C}^{N_s}$ is zero-mean complex circular AWGN having covariance matrix $\mathbb{E}[\mathbf{n}_s(i) \mathbf{n}_s^H(i)] = \sigma_{n_s}^2 \mathbf{I}_{N_s}$, which is statistically independent of noise samples in other symbol intervals and slots.

The overall data block used by the sensor to estimate the direction $\mathbf{d}_k = [\phi_k, \varphi_k]^T \in \mathbb{R}^2$ of the k -th outdoor user during the current time slot is given by

$$\mathbf{Y}_{s,k} \triangleq [\mathbf{y}_{s,k}(0), \mathbf{y}_{s,k}(1), \dots, \mathbf{y}_{s,k}(I_p-1)] \in \mathbb{C}^{N_s \times I_p} \\ = \alpha_k \mathbf{a}_S(\phi_k, \varphi_k) \mathbf{a}_{\text{STAR}}^H(\phi_k, \varphi_k) \Phi_R^p \mathbf{H}_1 \mathbf{W} \mathbf{S} + \mathbf{N}_s \quad (28)$$

with $\mathbf{S} \triangleq [\mathbf{s}(0), \mathbf{s}(1), \dots, \mathbf{s}(I_p-1)] \in \mathbb{C}^{K \times I_p}$ collecting the symbols transmitted during the preparation stage and the matrix $\mathbf{N}_s \triangleq [\mathbf{n}_s(0), \mathbf{n}_s(1), \dots, \mathbf{n}_s(I_p-1)] \in \mathbb{C}^{N_s \times I_p}$ gathering the corresponding noise samples. With reference to the k -th target, the *sensing signal-to-noise ratio* (SSNR) is defined as

$$\text{SSNR}_k = \frac{|\alpha_k|^2 \|\mathbf{a}_S(\phi_k, \varphi_k) \mathbf{a}_{\text{STAR}}^H(\phi_k, \varphi_k) \Phi_R^p \mathbf{H}_1 \mathbf{W}\|^2}{N_s \sigma_{n_s}^2} \quad (29)$$

for $k \in \mathcal{K}_R$. On the basis of the observations $\mathbf{Y}_{s,k}$, the task of the sensor is to provide an estimate $\hat{\mathbf{d}}_k = [\hat{\phi}_k, \hat{\varphi}_k]^T \in \mathbb{R}^2$ of the k -th outdoor direction during the current slot, which can be obtained by the classic maximum likelihood estimation (MLE) [31], [52] or subspace-based algorithms [53]–[55]. The mean square errors (MSEs) $\sigma_{\phi_k}^2 \triangleq \mathbb{E}[(\phi_k - \hat{\phi}_k)^2]$ and $\sigma_{\varphi_k}^2 \triangleq \mathbb{E}[(\varphi_k - \hat{\varphi}_k)^2]$ are commonly used to evaluate the estimation performance. The posterior Cramér–Rao bound (PCRB) [56] establishes a lower bound on $\sigma_{\phi_k}^2$ and $\sigma_{\varphi_k}^2$ and, hence, it is a rigorous benchmark for direction estimation accuracy. However, in STAR-RIS-enabled ISAC systems, the PCRB typically leads to highly intricate mathematical expressions [31].

Therefore, using the PCRB as performance metric significantly complicates the optimization problem and limits analytical tractability. To maintain a good balance between accuracy and computational simplicity, we adopt the SSNR as the primary performance indicator for the estimation of outdoor users' directions. This approach allows us to formulate the problem in a more tractable manner, while still capturing the essential impact of beamforming, propagation conditions, and STAR-RIS configuration on the achievable sensing performance. However, replacing the PCRB with the SSNR is meaningful primarily in the high-SSNR regime [56]. For this reason, we impose the sensing constraint $\mathbb{E}[\text{SSNR}_k] \geq \delta_{\text{sens}}$, with $\delta_{\text{sens}} > 0$ being a given threshold, which ensures operation in the high-SSNR region and makes the SSNR-based uncertainty model a reliable approximation.

III. OPTIMIZATION FRAMEWORK

We formulate an optimization problem, aimed at maximizing the achievable communication rate with respect to \mathbf{W} , Φ_R^p (encompassing \mathbf{b} too), Φ_T^p , Φ_R^c , and Φ_T^c , while ensuring that both the BS transmit power constraint and the target detection performance requirement are satisfied. The considered optimization also takes into account the intrinsic physical limitations of the STAR-RIS elements, such as energy conservation, amplitude-phase coupling, and power-splitting constraints between transmission and reflection modes.

According to (11), the matrix Φ_R^p depends on both the metasurface partition vector \mathbf{b} and the STAR-RIS reflection coefficients during the preparation phase. For optimization purposes, we exploit the factorization $\Phi_R^p = \mathbf{B} \tilde{\Phi}_R^p$, where $\mathbf{B} = \text{diag}(\mathbf{b})$ encodes the metasurface partition, while $\tilde{\Phi}_R^p \triangleq \text{diag}(\tilde{\beta}_{R,1}^p e^{j\theta_{R,1}^p}, \tilde{\beta}_{R,2}^p e^{j\theta_{R,2}^p}, \dots, \tilde{\beta}_{R,N}^p e^{j\theta_{R,N}^p})$ contains only the reflection amplitudes and phases of the STAR-RIS during the preparation stage.

A key observation is that, for $k \in \mathcal{K}_R$ and $v \in \{p,c\}$, the SINR in (23) depends on the direction \mathbf{d}_k of the outdoor users and, thus, knowledge of \mathbf{d}_k is required to jointly design the transmit beamforming at the BS and the transmission/reflection coefficients at the STAR-RIS during both the preparation and communication phases. In practice, the directions of outdoor users typically vary in a very slow manner compared to the slot duration T , as their spatial positions change only slightly over short time intervals. This is especially true in scenarios with moderate user mobility or quasi-static targets. As a result, the outdoor directions remain approximately constant between two adjacent time slots and, consequently, their estimates during a slot can be reliably reused for system design in the preparation phase of the subsequent slot.

Hereinafter, for $k \in \mathcal{K}_R$, we denote with ϕ_k^p and φ_k^p the angles of the outdoor users used to optimize the system during the preparation phase: they correspond to the direction estimates of the outdoor users obtained in the previous slot. On the other hand, for $k \in \mathcal{K}_R$, the system design during the communication phase relies on the outdoor user angles ϕ_k^c and φ_k^c , estimated in the preparation stage of the same slot. Specifically, with reference to the t -th slot, we set

$\phi_k^p = \hat{\phi}_k(t-1)$ and $\varphi_k^p = \hat{\varphi}_k(t-1)$ in the preparation phase, and $\phi_k^c = \hat{\phi}_k(t)$ and $\varphi_k^c = \hat{\varphi}_k(t)$ in the communication stage.

To enhance robustness against estimation errors of the outdoor users' directions, we average the achievable rate and the SSNR with respect to the random variables $\epsilon_{\phi_k}^v \triangleq \phi_k - \phi_k^v$ and $\epsilon_{\varphi_k}^v \triangleq \varphi_k - \varphi_k^v$, for $k \in \mathcal{K}_R$ and $v \in \{p,c\}$. The optimization problem can thus be formulated as

$$(\mathbf{P1}) \quad \max_{\mathbf{W}, \tilde{\Phi}_R^p, \mathbf{b}, \Phi_T^p, \Phi_R^c, \Phi_T^c} \mathbb{E}[\mathcal{R}] \quad (30a)$$

$$\text{s.t. } \phi_k = \phi_k^p + \epsilon_{\phi_k}^p, \varphi_k = \varphi_k^p + \epsilon_{\varphi_k}^p \quad (30b)$$

$$\text{for } k \in \mathcal{K}_R \text{ and } i \in \{0, 1, \dots, I_p - 1\} \quad (30b)$$

$$\phi_k = \phi_k^c + \epsilon_{\phi_k}^c, \varphi_k = \varphi_k^c + \epsilon_{\varphi_k}^c \quad (30c)$$

$$\text{for } k \in \mathcal{K}_R \text{ and } i \in \{I_p, I_p + 1, \dots, I - 1\} \quad (30c)$$

$$\theta_{R,n}^v, \theta_{T,n}^v \in [0, 2\pi), \cos(\theta_{R,n}^v - \theta_{T,n}^v) = 0 \quad (30d)$$

$$\beta_{R,n}^v, \beta_{T,n}^v \in [0, 1], (\beta_{R,n}^v)^2 + (\beta_{T,n}^v)^2 = 1 \quad (30d)$$

$$\text{for } n \in \mathcal{N} \text{ and } v \in \{p,c\} \quad (30d)$$

$$\mathbb{E}[\text{SSNR}(\mathbf{d}_k)] \geq \delta_{\text{sens}}, \text{ for } k \in \mathcal{K}_R \quad (30e)$$

$$\mathcal{P} \leq \mathcal{P}_{\max} \quad (30f)$$

$$\|\mathbf{b}\|_1 = N_{\text{part}} \leq N \quad (30g)$$

where (30b) and (30c) account for the fact that the optimization relies on the estimates of the outdoor users' directions, with the expectation taken with respect to the estimation errors $\epsilon_{\phi_k}^v$ and $\epsilon_{\varphi_k}^v$, for $k \in \mathcal{K}_R$ and $v \in \{p,c\}$. Constraint (30d) ensures compliance with the physical operating conditions of the STAR-RIS, constraint (30e) guarantees that the average SSNR (ASSNR) of the targets remains above a given threshold δ_{sens} , and is active only during the preparation phase, constraint (30f) ensures that the BS transmission power does not exceed its maximum limit $\mathcal{P}_{\max} > 0$, and, finally, constraint (30g) partitions the STAR-RIS during the preparation phase, with N_{part} elements operating in ES mode and the others in transmit-only mode.

A. Evaluation of the average performance metrics

To calculate the average achievable rate and the average sensing SNR, we assume that the random pairs $(\epsilon_{\phi_{K_T+1}}^v, \epsilon_{\varphi_{K_T+1}}^v), (\epsilon_{\phi_{K_T+2}}^v, \epsilon_{\varphi_{K_T+2}}^v), \dots, (\epsilon_{\phi_K}^v, \epsilon_{\varphi_K}^v)$ are statistically independent, with $v \in \{p,c\}$. For high SNR and large samples, DOA estimates from MLE and subspace-based algorithms are asymptotically normal with variance approaching the PCRB [56], [57]. Therefore, for each $k \in \mathcal{K}_R$, the estimation errors $\epsilon_{\phi_k}^v$ and $\epsilon_{\varphi_k}^v$ are modeled as independent zero-mean Gaussian random variables with variance $\sigma_{\phi_k}^2$ and $\sigma_{\varphi_k}^2$ given by the corresponding PCRB, whose expression can be found in [31].

It is worth noting that the estimates ϕ_k^p and φ_k^p used in the current slot were obtained during the previous slot. Consequently, they are treated as deterministic parameters in the optimization performed during the preparation stage. Likewise, ϕ_k^c and φ_k^c have been acquired in the preparation phase of the current slot and they are therefore regarded as deterministic quantities in the subsequent communication-stage optimization. Consequently, the angles ϕ_k and φ_k of the

outdoor users in (30b) and (30c) are independent Gaussian random variables with mean ϕ_k^v and φ_k^v , and variance $\sigma_{\phi_k}^2$ and $\sigma_{\varphi_k}^2$, respectively, for all $k \in \mathcal{K}_R$ and $v \in \{p, c\}$.

It comes from (24) that

$$\mathbb{E}[\mathcal{R}] = \eta \mathbb{E}[\mathcal{R}^p] + (1 - \eta) \mathbb{E}[\mathcal{R}^c] \quad (31)$$

where, by virtue of (23) and (25), one obtains

$$\begin{aligned} \mathbb{E}[\mathcal{R}^v] &= \sum_{k=1}^{K_T} \log_2 (1 + \gamma_k^v) \\ &+ \sum_{k=K_T+1}^K \mathbb{E}[\log_2 (1 + \gamma_k^v)] \leq \bar{\mathcal{R}}_{\max}^v \end{aligned} \quad (32)$$

with

$$\bar{\mathcal{R}}_{\max}^v \triangleq \sum_{k=1}^{K_T} \log_2 (1 + \gamma_k^v) + \sum_{k=K_T+1}^K \log_2 (1 + \mathbb{E}[\gamma_k^v]) \quad (33)$$

for $v \in \{p, c\}$, where the upper bound follows from the application of Jensen's inequality [52]. The exact expression of $\mathbb{E}[\gamma_k^v]$ is intractable due to the nonlinear ratio of random functions. To obtain a tractable yet accurate characterization, we employ a first-order approximation [58] by replacing the random ratio with the ratio of the corresponding expectations:

$$\begin{aligned} \mathbb{E}[\gamma_k^v] &\approx \frac{\mathbb{E} \left[\left| \{\mathbf{h}_{2,k}^v\}^H \Phi^v(k) \mathbf{H}_1 \mathbf{w}_k \right|^2 \right]}{\sum_{\substack{h=1 \\ h \neq k}}^K \mathbb{E} \left[\left| \{\mathbf{h}_{2,k}^v\}^H \Phi^v(k) \mathbf{H}_1 \mathbf{w}_h \right|^2 \right] + \sigma_{n_u}^2} \\ &= \frac{\mathbf{w}_k^H \mathbf{H}_1^H \{\Phi^v(k)\}^* \mathbf{R}_{\mathbf{h}_{2,k} \mathbf{h}_{2,k}}^v \Phi^v(k) \mathbf{H}_1 \mathbf{w}_k}{\sum_{\substack{h=1 \\ h \neq k}}^K \mathbf{w}_h^H \mathbf{H}_1^H \{\Phi^v(k)\}^* \mathbf{R}_{\mathbf{h}_{2,k} \mathbf{h}_{2,k}}^v \Phi^v(k) \mathbf{H}_1 \mathbf{w}_h + \sigma_{n_u}^2} \end{aligned} \quad (34)$$

for $k \in \mathcal{K}_R$, where $\mathbf{R}_{\mathbf{h}_{2,k} \mathbf{h}_{2,k}}^v \triangleq \mathbb{E} \left[\mathbf{h}_{2,k}^v \{\mathbf{h}_{2,k}^v\}^H \right]$ and, according to (16), one has

$$\begin{aligned} \{\mathbf{h}_{2,k}^v\}^H &= \sqrt{\varsigma_{\text{out},k}} \left(\sqrt{\frac{\mu_{2,\text{out}}}{1 + \mu_{2,\text{out}}}} \right. \\ &\quad \cdot \mathbf{a}_{\text{STAR}}^H(\phi_k^v + \epsilon_{\phi_k}^v, \varphi_k^v + \epsilon_{\varphi_k}^v) \\ &\quad \left. + \sqrt{\frac{1}{1 + \mu_{2,\text{out}}}} \{\mathbf{h}_{2,k}^{\text{NLoS}}\}^H \right) \end{aligned} \quad (35)$$

with $\{\mathbf{h}_{2,k}^{\text{NLoS}}\}^H$ being the k -th row of the matrix $\mathbf{H}_2^{\text{NLoS}}$, for $k \in \mathcal{K}_R$ and $v \in \{p, c\}$. The approximation in (34) is accurate when the fluctuations of the numerator and denominator around their means are small compared to their average values. Generally, the correlation matrix $\mathbf{R}_{\mathbf{h}_{2,k} \mathbf{h}_{2,k}}^v$ does not admit a simple closed form due to the nonlinear dependence of the STAR-RIS steering vector on the errors $\epsilon_{\phi_k}^v$ and $\epsilon_{\varphi_k}^v$, as it is clear from (18). In the simulations of Section IV, given ϕ_k^v , φ_k^v , $\sigma_{\phi_k}^2$, and $\sigma_{\varphi_k}^2$, the matrix $\mathbf{R}_{\mathbf{h}_{2,k} \mathbf{h}_{2,k}}^v$ is evaluated numerically.

The ASSNR comes from averaging (29) with respect to $\epsilon_{\phi_k}^p$ and $\epsilon_{\varphi_k}^p$, thus yielding

$$\begin{aligned} \mathbb{E}[\text{SSNR}(\mathbf{d}_k)] &= \frac{|\alpha_k|^2}{N_s \sigma_{n_s}^2} \mathbb{E} \left[\left\| \mathbf{a}_S(\phi_k^p + \epsilon_{\phi_k}^p, \varphi_k^p + \epsilon_{\varphi_k}^p) \right. \right. \\ &\quad \cdot \mathbf{a}_{\text{STAR}}^H(\phi_k^p + \epsilon_{\phi_k}^p, \varphi_k^p + \epsilon_{\varphi_k}^p) \Phi_R^p \mathbf{H}_1 \mathbf{W} \left. \left. \right\|^2 \right] \\ &= \frac{|\alpha_k|^2}{N_s \sigma_{n_s}^2} \text{tr} \left[\mathbf{W}^H \mathbf{H}_1^H \{\Phi_R^p\}^* \mathbf{R}_{\mathbf{a}_{\text{STAR}},k}^p \Phi_R^p \mathbf{H}_1 \mathbf{W} \right] \end{aligned} \quad (36)$$

for $k \in \mathcal{K}_R$, with

$$\begin{aligned} \mathbf{R}_{\mathbf{a}_{\text{STAR}},k}^p &\triangleq \mathbb{E} \left[\left\| \mathbf{a}_S(\phi_k^p + \epsilon_{\phi_k}^p, \varphi_k^p + \epsilon_{\varphi_k}^p) \right\|^2 \right. \\ &\quad \cdot \mathbf{a}_{\text{STAR}}^H(\phi_k^p + \epsilon_{\phi_k}^p, \varphi_k^p + \epsilon_{\varphi_k}^p) \mathbf{a}_{\text{STAR}}^H(\phi_k^p + \epsilon_{\phi_k}^p, \varphi_k^p + \epsilon_{\varphi_k}^p) \left. \right] \end{aligned} \quad (37)$$

under (30b) and (30c). Similarly to $\mathbf{R}_{\mathbf{h}_{2,k} \mathbf{h}_{2,k}}^v$, the matrix $\mathbf{R}_{\mathbf{a}_{\text{STAR}},k}^p$ cannot be expressed in closed form and, hence, it is calculated by means of numerical techniques in Section IV.

B. Closed-form fractional programming solution

In the sequel, we consider a modification of problem **(P1)**, which is obtained by replacing $\mathbb{E}[\mathcal{R}^v]$ in (31) with $\bar{\mathcal{R}}_{\max}^v$ given by (33), where $\mathbb{E}[\gamma_k^v]$ is approximated as in (34), for $v \in \{p, c\}$ and $k \in \mathcal{K}_R$. In a unified form, we rewrite $\bar{\mathcal{R}}_{\max}^v$ as

$$\bar{\mathcal{R}}_{\max}^v = \sum_{k=1}^K \log_2 (1 + \bar{\gamma}_k^v) \quad (38)$$

where

$$\bar{\gamma}_k^v \triangleq \frac{\mathbf{w}_k^H \mathbf{H}_1^H \{\Phi^v(k)\}^* \mathbf{R}^v(k) \Phi^v(k) \mathbf{H}_1 \mathbf{w}_k}{\sum_{\substack{h=1 \\ h \neq k}}^K \mathbf{w}_h^H \mathbf{H}_1^H \{\Phi^v(k)\}^* \mathbf{R}^v(k) \Phi^v(k) \mathbf{H}_1 \mathbf{w}_h + \sigma_{n_u}^2} \quad (39)$$

with

$$\mathbf{R}^v(k) \triangleq \begin{cases} \mathbf{h}_{2,k}^v \{\mathbf{h}_{2,k}^v\}^H, & \text{for } k \in \mathcal{K}_T \\ \mathbf{R}_{\mathbf{h}_{2,k} \mathbf{h}_{2,k}}^v, & \text{for } k \in \mathcal{K}_R \end{cases} \quad (40)$$

We refer to such an optimization problem as **(P1-mod)**. This problem is difficult to solve because it is non-convex due to the coupling between the variables, as well as to the non-linear sensing constraint. Further, the optimization variables are mixed discrete-continuous.

Herein, we apply fractional programming (FP) theory [59], [60] to derive an equivalent yet more tractable fractional formulation. More precisely, we resort to closed-form FP. Such an approach relies on a Lagrangian dual reformulation of the original problem, enabling an algorithm where each iteration admits a closed-form update instead of requiring the numerical solution of a convex subproblem as in the direct FP alternative [59], [60]. The Lagrangian dual transform is capable of converting the cost function of problem **(P1-mod)** to a sum-of-ratio form. Specifically, let $\bar{\tau}^v \triangleq [\bar{\tau}_1^v, \bar{\tau}_2^v, \dots, \bar{\tau}_K^v]^T \in \mathbb{R}^K$ be a vector of auxiliary variables, for $v \in \{p, c\}$, problem **(P1-mod)** is equivalent to maximizing (see [60] for a constructive proof)

$$\bar{\mathcal{R}} = \eta \bar{\mathcal{R}}^p + (1 - \eta) \bar{\mathcal{R}}^c \quad (41)$$

$$\bar{\mathcal{R}}^v \triangleq \sum_{k=1}^K \log_2 (1 + \bar{\tau}_k^v) - \sum_{k=1}^K \bar{\tau}_k^v + \sum_{k=1}^K \underbrace{\frac{(1 + \bar{\tau}_k^v) \mathbf{w}_k^H \mathbf{H}_1^H \{\Phi^v(k)\}^* \mathbf{R}^v(k) \Phi^v(k) \mathbf{H}_1 \mathbf{w}_k}{\sum_{h=1}^K \mathbf{w}_h^H \mathbf{H}_1^H \{\Phi^v(k)\}^* \mathbf{R}^v(k) \Phi^v(k) \mathbf{H}_1 \mathbf{w}_h + \sigma_{n_u}^2}}_{\text{Sum-of-ratio term}} \quad (42)$$

$$\begin{aligned} \bar{\mathcal{R}}_q^v = & \sum_{k=1}^K \log_2 (1 + \bar{\tau}_k^v) - \sum_{k=1}^K \bar{\tau}_k^v + \sum_{k=1}^K 2 \bar{\rho}_k^v \sqrt{(1 + \bar{\tau}_k^v) \mathbf{w}_k^H \mathbf{H}_1^H \{\Phi^v(k)\}^* \mathbf{R}^v(k) \Phi^v(k) \mathbf{H}_1 \mathbf{w}_k} \\ & - \sum_{k=1}^K (\bar{\rho}_k^v)^2 \left(\sum_{h=1}^K \mathbf{w}_h^H \mathbf{H}_1^H \{\Phi^v(k)\}^* \mathbf{R}^v(k) \Phi^v(k) \mathbf{H}_1 \mathbf{w}_h + \sigma_{n_u}^2 \right) \end{aligned} \quad (44)$$

with respect to (w.r.t.) $\mathbf{W}, \tilde{\Phi}_R^p, \mathbf{b}, \Phi_T^p, \Phi_R^c, \Phi_T^c, \bar{\tau}^p, \bar{\tau}^c$, s.t. (30b), (30c), (30d), (30e), (30f), and (30g), where $\bar{\mathcal{R}}^v$ is reported in (42) at the top of the next page, for $v \in \{p, c\}$. The equivalence between the two problems stems from the fact that $\bar{\mathcal{R}}$ is a concave differentiable function over $\bar{\tau}^p$ and $\bar{\tau}^c$, when $\mathbf{W}, \tilde{\Phi}_R^p, \mathbf{b}, \Phi_T^p, \Phi_R^c, \Phi_T^c$ are held fixed. In this case, the optimal value of $\bar{\tau}_k^v$ is obtained by setting $\partial \bar{\mathcal{R}} / \partial \bar{\tau}_k^v = 0$, thus yielding

$$\bar{\tau}_{k,\text{opt}}^v = \bar{\gamma}_k^v \quad (43)$$

for $v \in \{p, c\}$ and $k \in \mathcal{K}$. It is worth noticing that the optimal $\bar{\tau}_k^v$ is equal to the downlink SINR of the k -th user. On the other hand, when $\bar{\tau}^v$ is kept fixed, only the last term of $\bar{\mathcal{R}}^v$ in (42), which has a sum-of-ratio form, is involved in the optimization of the variables $\mathbf{W}, \tilde{\Phi}_R^p, \mathbf{b}, \Phi_T^p, \Phi_R^c, \Phi_T^c$. By the quadratic transform [59], [60] on the fractional term in (42), we may further recast $\bar{\mathcal{R}}^v$ as reported in (44) at the top of the next page, where $\bar{\rho}^v \triangleq [\bar{\rho}_1^v, \bar{\rho}_2^v, \dots, \bar{\rho}_K^v]^T \in \mathbb{R}^K$ is a vector of auxiliary variables. Hence, to optimize the variables $\mathbf{W}, \tilde{\Phi}_R^p, \mathbf{b}, \Phi_T^p, \Phi_R^c, \Phi_T^c$, we can equivalently maximize (see [60, Corollary 1] for the formal proof)

$$\bar{\mathcal{R}}_q = \eta \bar{\mathcal{R}}_q^p + (1 - \eta) \bar{\mathcal{R}}_q^c \quad (45)$$

w.r.t. $\mathbf{W}, \tilde{\Phi}_R^p, \mathbf{b}, \Phi_T^p, \Phi_R^c, \Phi_T^c, \bar{\rho}^p, \bar{\rho}^c$, s.t. (30b), (30c), (30d), (30e), (30f), and (30g), where the entries of $\bar{\tau}^v$ are iteratively optimized according to (43), for $v \in \{p, c\}$. When all the other variables are fixed, the optimal value of $\bar{\rho}_k^v$ can be obtained by setting $\partial \bar{\mathcal{R}}_q / \partial \bar{\rho}_k^v = 0$, i.e.,

$$\bar{\rho}_{k,\text{opt}}^v = \frac{\sqrt{(1 + \bar{\tau}_k^v) \mathbf{w}_k^H \mathbf{H}_1^H \{\Phi^v(k)\}^* \mathbf{R}^v(k) \Phi^v(k) \mathbf{H}_1 \mathbf{w}_k}}{\sum_{h=1}^K \mathbf{w}_h^H \mathbf{H}_1^H \{\Phi^v(k)\}^* \mathbf{R}^v(k) \Phi^v(k) \mathbf{H}_1 \mathbf{w}_h + \sigma_{n_u}^2}. \quad (46)$$

In the forthcoming subsections, we develop the optimization of the variables $\mathbf{W}, \tilde{\Phi}_R^p, \mathbf{b}, \Phi_T^p, \Phi_R^c, \Phi_T^c$ in the preparation and communication phases, by fixing $\bar{\tau}^v$ and $\bar{\rho}^v$, for $v \in \{p, c\}$.

C. Optimization of the beamforming matrix at the BS

This subsection focuses on optimizing the BS beamformer, while keeping $\Phi_R^v, \Phi_T^v, \bar{\tau}^v, \bar{\rho}^v$ fixed, for a given system's stage

$v \in \{p, c\}$. The problem to be solved reads as

$$(\mathbf{P2}) : \max_{\mathbf{W}} \bar{\mathcal{R}}_q^v \quad (47a)$$

$$\text{s.t. } \mathbb{E}[\text{SSNR}(\mathbf{d}_k)] \geq \delta_{\text{sens}}, \text{ for } k \in \mathcal{K}_R \quad (47b)$$

$$\mathcal{P} \leq \mathcal{P}_{\max} \quad (47c)$$

where the transformed objective $\bar{\mathcal{R}}_q^v$ is concave in \mathbf{W} . According to (2), the convex constraint (47c) is explicated as

$$\sum_{h=1}^K \mathbf{w}_h^H \mathbf{w}_h \leq \mathcal{P}_{\max}. \quad (48)$$

It is worth noting that the beamforming matrix has to be optimized in both stages of the protocol: during the preparation phase, where it jointly supports communication and direction estimation, and again in the communication phase, where the updated angular information is exploited to refine the communication process.

During the communication phase, constraint (47b) is removed and, thus, problem **(P2)** reduces to a communication-only beamforming design under a sum transmit power constraint [61]. In this stage, the resulting problem is convex and satisfies Slater's condition [58], [62]. Consequently, strong duality holds and the Karush–Kuhn–Tucker (KKT) conditions are necessary and sufficient for optimality.

The solution of problem **(P2)** is more challenging during the preparation phase, when constraint (47b) is active. In this stage, relying on (36), constraint (47b) can be rewritten as

$$f_k(\mathbf{W}) \triangleq \sum_{h=1}^K \mathbf{w}_h^H \mathbf{P}_k \mathbf{w}_h \geq \frac{\delta_{\text{sens}} N_s \sigma_{n_s}^2}{|\alpha_k|^2} \quad (49)$$

with $\mathbf{P}_k \triangleq \mathbf{H}_1^H \{\Phi_R^p\}^* \mathbf{R}_{\text{as}, \text{STAR}, k}^p \Phi_R^p \mathbf{H}_1 \in \mathbb{C}^{M \times M}$, which is active only during the preparation phase. The sensing constraint in (49) is non-convex because it involves a super-level set of a convex quadratic form. To handle this, we adopt a successive convex approximation (SCA) strategy [63].

At iteration $i \in \mathbb{N}_0$, let $\mathbf{W}^i \triangleq [\mathbf{w}_1^i, \mathbf{w}_2^i, \dots, \mathbf{w}_K^i]$ be the current beamformer matrix. The first-order Taylor expansion of $f_k(\mathbf{W})$ around \mathbf{W}^i gives a global affine lower bound

$$f_k(\mathbf{W}) \geq \sum_{h=1}^K 2 \Re \{ [\mathbf{w}_h^i]^H \mathbf{P}_k \mathbf{w}_h \} - \sum_{h=1}^K [\mathbf{w}_h^i]^H \mathbf{P}_k \mathbf{w}_h^i. \quad (50)$$

Therefore, at iteration $i+1$, we may replace (49) with its affine inner approximation

$$\sum_{h=1}^K 2 \Re \{ [\mathbf{w}_h^i]^H \mathbf{P}_k \mathbf{w}_h \} - \sum_{h=1}^K [\mathbf{w}_h^i]^H \mathbf{P}_k \mathbf{w}_h^i \geq \frac{\delta_{\text{sens}} N_s \sigma_{n_s}^2}{|\alpha_k|^2} \quad (51)$$

for $k \in \mathcal{K}_R$. Such a set of constraints is convex and still inner-approximates the original feasible set, ensuring monotonic improvement under standard SCA conditions [63]. Consequently, at iteration $i+1$, the maximization of $\bar{\mathcal{R}}_q^p$ w.r.t. \mathbf{W} , s.t. (48) and (51), is a convex quadratically constrained quadratic program (QCQP), which can be handled with standard solvers [58]. The corresponding solution \mathbf{W}^{i+1} is then updated and the algorithm is repeated until convergence.

D. Optimization of the STAR-RIS partition during the preparation phase

In this subsection, we tackle the optimization of the binary selection vector \mathbf{b} during the preparation phase, when \mathbf{W} , $\tilde{\Phi}_R^p$, Φ_T^p , $\bar{\tau}^p$, $\bar{\rho}^p$ are kept fixed. We recall that, during the communication phase, all the elements of the STAR-RIS work in ES mode, i.e., $\mathbf{b} = \mathbf{1}_N$. In the preparation stage, the optimization problem assumes the form

$$(\mathbf{P3}) : \max_{\mathbf{b} \in \{0,1\}^N} \bar{\mathcal{R}}_q^p \quad (52a)$$

$$\text{s.t. } \|\mathbf{b}\|_1 = N_{\text{part}} \leq N. \quad (52b)$$

Optimization (P3) is a purely combinatorial problem and, therefore, SCA cannot be applied *directly* in its original form. To circumvent such a problem, we propose to first relax the binary constraint by replacing $\mathbf{b} \in \{0,1\}^N$ with its continuous approximation $\mathbf{b} \in [0,1]^N$ and, then, enforce a “binary-like” behavior via a penalty term

$$\chi \triangleq \sum_{n=1}^N (b_n - b_n^2) \quad (53)$$

which is maximized when $b_n = 0$ or $b_n = 1$. Specifically, we consider the penalized objective $\bar{\mathcal{R}}_{q,\text{pen}}^p \triangleq \bar{\mathcal{R}}_q^p - \kappa \chi$, which is maximized w.r.t. $\mathbf{b} \in [0,1]^N$, where κ is the regularization parameter. Such an optimization problem is non-convex, since χ is the difference of convex mappings (a linear function minus a convex quadratic one) and it can be now solved by leveraging SCA. At iteration $i+1$, by resorting to first-order Taylor expansion, we linearize the concave part $-b_n^2$ of χ around the current point b_n^i , thus obtaining $-b_n^2 \approx -(b_n^i)^2 - 2b_n^i(b_n - b_n^i)$, which yields the affine approximation of the penalty term

$$\chi \approx \sum_{n=1}^N [b_n - (b_n^i)^2 - 2b_n^i(b_n - b_n^i)]. \quad (54)$$

With this first-order linearization, the subproblem at iteration $i+1$, which amounts to maximize $\bar{\mathcal{R}}_{q,\text{pen}}^p$ w.r.t. \mathbf{b} with the approximation (54), becomes convex and can be tackled with a standard convex solver [58]. The resulting solution $\mathbf{b}^{i+1} \triangleq [b_1^{i+1}, b_2^{i+1}, \dots, b_N^{i+1}]^T \in [0,1]^N$ is then updated and the process is repeated until convergence.

Finally, to enforce the constraint (52b) and binarize the vector obtained after convergence of the SCA algorithm, the

binary partition vector $\mathbf{b} \in \{0,1\}^N$ is obtained by selecting the N_{part} entries of largest magnitude and setting them to one, while the remaining elements are set to zero. This operation constitutes the Euclidean projection onto the feasible binary set with fixed cardinality.

E. Optimization of the STAR-RIS coefficients

In this subsection, we tackle the optimization of the STAR-RIS parameters, while maintaining \mathbf{W} , \mathbf{b} , $\bar{\tau}^v$, and $\bar{\rho}^v$ fixed, for a given system’s stage $v \in \{p,c\}$. In this case, we have to solve the following optimization problem

$$(\mathbf{P4}) : \max_{\tilde{\Phi}_R^v, \Phi_T^v} \bar{\mathcal{R}}_q^v \quad (55a)$$

$$\text{s.t. } \theta_{R,n}^v, \theta_{T,n}^v \in [0, 2\pi], \cos(\theta_{R,n}^v - \theta_{T,n}^v) = 0 \\ \beta_{R,n}^v, \beta_{T,n}^v \in [0, 1], (\beta_{R,n}^v)^2 + (\beta_{T,n}^v)^2 = 1, \forall n \in \mathcal{N} \quad (55b)$$

$$\mathbb{E}[\text{SSNR}(\mathbf{d}_k)] \geq \delta_{\text{sens}}, \text{ for } k \in \mathcal{K}_R. \quad (55c)$$

with $\tilde{\Phi}_R^v = \Phi_R^v$ as defined in (13). In this case, the transformed objective function $\bar{\mathcal{R}}_q^v$ in (44) depends on the STAR-RIS coefficients only through quadratic forms of the reflection and transmission coefficient vectors. Specifically, let

$$\phi_R^p \triangleq [b_1 \tilde{\beta}_{R,1}^p e^{j\theta_{R,1}^p}, b_2 \tilde{\beta}_{R,2}^p e^{j\theta_{R,2}^p}, \dots, b_N \tilde{\beta}_{R,N}^p e^{j\theta_{R,N}^p}]^T \quad (56)$$

$$\phi_T^p \triangleq [\beta_{T,1}^p e^{j\theta_{T,1}^p}, \beta_{T,2}^p e^{j\theta_{T,2}^p}, \dots, \beta_{T,N}^p e^{j\theta_{T,N}^p}]^T \quad (57)$$

$$\phi_a^c \triangleq [\beta_{a,1}^c e^{j\theta_{a,1}^c}, \beta_{a,2}^c e^{j\theta_{a,2}^c}, \dots, \beta_{a,N}^c e^{j\theta_{a,N}^c}]^T \quad (58)$$

for $a \in \{T, R\}$. By using the cyclic property of the trace operator [64] and element-wise matrix multiplication,¹ the objective function in (44) can be written as reported in (59) at the top of the next page, where $\mathbf{E}_{k,h}^v \triangleq \mathbf{R}^v(k) \odot (\mathbf{H}_1 \mathbf{w}_h \mathbf{w}_h^H \mathbf{H}_1^H)^T \in \mathbb{C}^{N \times N}$. Similarly, we may rewrite the ASSNR in (36) as

$$\mathbb{E}[\text{SSNR}(\mathbf{d}_k)] = \frac{|\alpha_k|^2}{N_s \sigma_{n_s}^2} \{ \phi_R^p \}^H \mathbf{D}_k^p \phi_R^p, \quad \text{for } k \in \mathcal{K}_R \quad (60)$$

with $\mathbf{D}_k^p \triangleq \mathbf{R}_{\mathbf{a}, \mathbf{a}_{\text{STAR}}, k}^p \odot (\mathbf{H}_1 \mathbf{W} \mathbf{W}^H \mathbf{H}_1^H)^T \in \mathbb{C}^{N \times N}$. Since \mathbf{D}_k^p is a positive semidefinite (PSD) matrix, the quadratic form in (60) is convex in ϕ_R^p . However, its upper level set is not necessarily convex. As a result, problem (P4) is non-convex and requires additional techniques to be effectively solved.

To convexify the problem, we follow a semidefinite relaxation (SDR) approach [58], [62] by introducing the rank-one PSD matrix $\mathbf{V}_a^v \triangleq \phi_a^v \{ \phi_a^v \}^H \succeq 0$, for $a \in \{T, R\}$ and $v \in \{p,c\}$. As a consequence, using again the cyclic property of the trace operator, the quadratic terms in (59) and (60) become $\{ \phi_a^v \}^H \mathbf{E}_{k,h}^v \phi_a^v = \text{tr}(\mathbf{E}_{k,h}^v \mathbf{V}_a^v)$ and $\{ \phi_R^p \}^H \mathbf{D}_k^p \phi_R^p = \text{tr}(\mathbf{D}_k^p \mathbf{V}_R^p)$, respectively, which are linear in the lifted matrix \mathbf{V}_a^v . The STAR-RIS physical constraints can be translated into affine constraints in the lifted variables. Indeed, it is verified that the diagonal entries of \mathbf{V}_a^v represent squared amplitudes $\{\mathbf{V}_a^v\}_{n,n} = (\beta_{a,n}^v)^2$, for each $n \in \mathcal{N}$. Since the

¹For vectors \mathbf{x} and \mathbf{y} , and corresponding diagonal matrices \mathbf{D}_x and \mathbf{D}_y with these vectors as their main diagonals, it holds (see, e.g., [64]) that $\mathbf{x}^H(\mathbf{A} \odot \mathbf{B}) \mathbf{y} = \text{tr}(\mathbf{D}_x^* \mathbf{A} \mathbf{D}_y \mathbf{B}^T)$.

$$\begin{aligned} \bar{\mathcal{R}}_q^v = & \sum_{k=1}^K \log_2 (1 + \bar{\tau}_k^v) - \sum_{k=1}^K \bar{\tau}_k^v + \sum_{k=1}^{K_T} 2 \bar{\rho}_k^v \sqrt{(1 + \bar{\tau}_k^v) \{\phi_T^v\}^H \mathbf{E}_{k,k}^v \phi_T^v} + \sum_{k=K_T+1}^K 2 \bar{\rho}_k^v \sqrt{(1 + \bar{\tau}_k^v) \{\phi_R^v\}^H \mathbf{E}_{k,k}^v \phi_R^v} \\ & - \sum_{k=1}^{K_T} (\bar{\rho}_k^v)^2 \left(\sum_{h=1}^K \{\phi_T^v\}^H \mathbf{E}_{k,h}^v \phi_T^v + \sigma_{n_u}^2 \right) - \sum_{k=K_T+1}^K (\bar{\rho}_k^v)^2 \left(\sum_{h=1}^K \{\phi_R^v\}^H \mathbf{E}_{k,h}^v \phi_R^v + \sigma_{n_u}^2 \right) \end{aligned} \quad (59)$$

equality constraint $(\beta_{R,n}^v)^2 + (\beta_{T,n}^v)^2 = 1$ is non-convex when combined with the rank-one requirement, we adopt the convex relaxation $(\beta_{R,n}^v)^2 + (\beta_{T,n}^v)^2 \leq 1$, for each $n \in \mathcal{N}$ and $v \in \{p,c\}$, which can be compactly written as

$$\text{diag}(\mathbf{V}_T^v) + \text{diag}(\mathbf{V}_R^v) \leq \mathbf{1}_N \quad (61)$$

where the inequality is understood element-wise.

Since the term $\text{tr}(\mathbf{E}_{k,k}^v \mathbf{V}_a^v)$ in (59) appears under a square root, for $a \in \{T, R\}$ and $v \in \{p, c\}$, we introduce the auxiliary variables $z_{a,k}^v \geq 0$ with $(z_{a,k}^v)^2 \leq \text{tr}(\mathbf{E}_{k,k}^v \mathbf{V}_a^v)$, which is a rotated *second-order cone (SOC)* constraint [58]. So doing, the objective (59) is converted into a linear function of $z_{a,k}^v$ and trace-linear functions of the lifted matrix \mathbf{V}_a^v , i.e.,

$$\begin{aligned} \bar{\mathcal{R}}_q^v = & \sum_{k=1}^{K_T} 2 \bar{\rho}_k^v \sqrt{1 + \bar{\tau}_k^v} z_{T,k}^v + \sum_{k=K_T+1}^K 2 \bar{\rho}_k^v \sqrt{1 + \bar{\tau}_k^v} z_{R,k}^v \\ & - \sum_{k=1}^{K_T} \text{tr}(\mathbf{C}_k^v \mathbf{V}_T^v) - \sum_{k=K_T+1}^K \text{tr}(\mathbf{C}_k^v \mathbf{V}_R^v) \\ & + \text{const}(\bar{\tau}^v, \bar{\rho}^v) \end{aligned} \quad (62)$$

where

$$\mathbf{C}_k^v \triangleq (\bar{\rho}_k^v)^2 \sum_{h=1}^K \mathbf{E}_{k,h}^v \in \mathbb{C}^{N \times N} \quad (63)$$

and $\text{const}(\bar{\tau}^v, \bar{\rho}^v)$ refers to a constant term when $\bar{\tau}^v$ and $\bar{\rho}^v$ are fixed. By virtue of the Schur complement [64], the SOC constraint is guaranteed by the linear matrix inequality (LMI)

$$\begin{bmatrix} \text{tr}(\mathbf{E}_{k,k}^v \mathbf{V}_a^v) & z_{a,k}^v \\ z_{a,k}^v & 1 \end{bmatrix} \succeq 0, \quad \text{with } z_{a,k}^v \geq 0. \quad (64)$$

By relaxing the rank-one constraints on \mathbf{V}_a^v while preserving the PSD condition $\mathbf{V}_a^v \succeq 0$, we obtain the SDR problem

$$\begin{aligned} \text{(P4)-sdr :} \quad & \max_{\substack{\{z_{T,k}^v\}_{k=1}^K, \{z_{R,k}^v\}_{k=1}^K \\ \mathbf{V}_T^v, \mathbf{V}_R^v}} \bar{\mathcal{R}}_q^v \\ \text{s.t.} \quad & \mathbf{V}_T^v \succeq 0, \mathbf{V}_R^v \succeq 0 \end{aligned} \quad (65a)$$

$$\text{diag}(\mathbf{V}_T^v) + \text{diag}(\mathbf{V}_R^v) \leq \mathbf{1}_N \quad (65b)$$

$$\begin{bmatrix} \text{tr}(\mathbf{E}_{k,k}^v \mathbf{V}_a^v) & z_{a,k}^v \\ z_{a,k}^v & 1 \end{bmatrix} \succeq 0, \quad \text{with } z_{a,k}^v \geq 0 \quad (65c)$$

$$\text{tr}(\mathbf{D}_k^p \mathbf{V}_R^p) \geq \frac{\delta_{\text{sens}} N_s \sigma_{n_s}^2}{|\alpha_k|^2}, \quad \text{for } k \in \mathcal{K}_R. \quad (65d)$$

This problem is a standard SDP with LMI and affine constraints and can be solved efficiently via interior-point methods with polynomial complexity [58]. Let $\{z_{a,k}^{v*}\}_{k=1}^K$ and \mathbf{V}_T^{v*} denote a solution of **(P4)-sdr**, for $a \in \{T, R\}$ and $v \in \{p, c\}$, two

cases may occur. If $\text{rank}(\mathbf{V}_a^{v*}) = 1$, then $\mathbf{V}_a^{v*} = \phi_a^{v*} \{\phi_a^{v*}\}^H$, and the optimal STAR-RIS coefficients are obtained directly from the principal eigenvector of \mathbf{V}_a^{v*} . If $\text{rank}(\mathbf{V}_a^{v*}) > 1$, the relaxation is not tight. A feasible rank-one approximation can be constructed via principal eigenvector extraction, followed by normalization, or Gaussian randomization with projection onto the feasible STAR-RIS set.

After recovery of the STAR-RIS parameters, the phase-coupling constraint $\cos(\theta_{R,n}^v - \theta_{T,n}^v) = 0$ can be enforced by projecting the obtained phases onto orthogonal pairs, as explained in the forthcoming subsection.

F. Phase-coupling restoration via Euclidean projection

Since the optimal solution of **(P4)-sdr** does not necessarily preserve the phase-coupling structure, we enforce it by projecting the obtained solution onto the feasible STAR-RIS set. This is achieved by minimizing the Euclidean distance between the normalized reference vector and the feasible coefficients.

$$\text{(P5) :} \quad \min_{\Phi_R^v, \Phi_T^v} \|\Phi_R^v - \Phi_R^v\|_2^2 + \|\Phi_T^v - \Phi_T^v\|_2^2 \quad (66a)$$

$$\text{s.t.} \quad \theta_{R,n}^v, \theta_{T,n}^v \in [0, 2\pi], \cos(\theta_{R,n}^v - \theta_{T,n}^v) = 0 \quad (66b)$$

$$\beta_{R,n}^v, \beta_{T,n}^v \in [0, 1], (\beta_{R,n}^v)^2 + (\beta_{T,n}^v)^2 = 1 \quad (66c)$$

$$\forall n \in \mathcal{N}$$

where the diagonal matrix $\Phi_a^{v*} = \text{diag}(\phi_a^{v*})$ is obtained from the solution of **(P4)-sdr**. Constraint (66b) enforces a $\pi/2$ phase difference between transmission and reflection coefficients and is non-convex due to its discrete nature. However, since (66b) and (66c) independently govern phase and amplitude, the problem can be solved via alternating optimization.

Let the amplitudes $\beta_{R,n}^v$ and $\beta_{T,n}^v$ be fixed, $\forall n \in \mathcal{N}$, problem **(P4)-sdr** reduces to a projection onto the phase-coupled feasible set. The following Lagrangian formulation addresses this phase-only subproblem. Defining the unit-modulus complex variable $u_{a,n}^v \triangleq e^{j\theta_{a,n}^v}$ and the unit-modulus complex parameter $u_{a,n}^{v*} \triangleq e^{j\theta_{a,n}^{v*}}$ (given by the solution of **(P4)-sdr**), for $a \in \{T, R\}$ and $v \in \{p, c\}$, constraint (66b) is equivalent to the orthogonality condition $\Re\{u_{R,n}^v (u_{T,n}^v)^*\} = 0$. Introducing a real Lagrange multiplier λ , the Lagrangian of the phase-only subproblem can be written $\forall n \in \mathcal{N}$ as

$$\begin{aligned} \mathcal{L}(u_{R,n}^v, u_{T,n}^v) \triangleq & |u_{R,n}^{v*} - u_{R,n}^v|^2 + |u_{T,n}^{v*} - u_{T,n}^v|^2 \\ & + \lambda \Re\{u_{R,n}^v (u_{T,n}^v)^*\} \end{aligned} \quad (67)$$

Using Wirtinger calculus [65], the stationary conditions are

$$\frac{\partial \mathcal{L}}{\partial (u_{R,n}^v)^*} = (u_{R,n}^{v*} - u_{R,n}^v) + \frac{\lambda}{2} u_{T,n}^v = 0 \quad (68)$$

$$\frac{\partial \mathcal{L}}{\partial (u_{T,n}^v)^*} = (u_{T,n}^{v*} - u_{T,n}^v) + \frac{\lambda}{2} u_{R,n}^v = 0. \quad (69)$$

Let $\mu = -\lambda/2 \in \mathbb{R}$. For $\mu^2 \neq 1$, the solution of the system of equations (68)-(69) is given by

$$u_{R,n}^v = \frac{u_{R,n}^{v*} - \mu u_{T,n}^{v*}}{1 - \mu^2} \quad \text{and} \quad u_{T,n}^v = \frac{u_{T,n}^{v*} - \mu u_{R,n}^{v*}}{1 - \mu^2}. \quad (70)$$

Substituting (70) into the orthogonality constraint yields

$$\Re \left\{ \frac{(u_{R,n}^{v*} - \mu u_{T,n}^{v*})(u_{T,n}^{v*} - \mu u_{R,n}^{v*})^*}{(1 - \mu^2)^2} \right\} = 0 \quad (71)$$

which leads to the second-order equation $c_1 \mu^2 - c_2 \mu + c_1 = 0$, with $c_1 \triangleq \Re \{u_{R,n}^{v*} (u_{T,n}^{v*})^*\}$ and $c_2 \triangleq |u_{R,n}^{v*}|^2 + |u_{T,n}^{v*}|^2$, whose solutions can be expressed in closed-form as

$$\mu = \frac{c_2 \pm \sqrt{c_2^2 - 4c_1^2}}{2c_1}. \quad (72)$$

For each $n \in \mathcal{N}$, the optimal phases are then obtained as

$$\hat{\theta}_{R,n}^v = \arg(u_{R,n}^{v*} - \mu u_{T,n}^{v*}) \quad (73)$$

$$\hat{\theta}_{T,n}^v = \arg(u_{T,n}^{v*} - \mu u_{R,n}^{v*}) \quad (74)$$

where the root in (72) minimizing the objective is selected. If $c_1 = 0$, then $\mu = 0$ and the phases are already orthogonal.

Let us now consider the derivation of the optimal amplitudes, for a given value of the phases $\theta_{R,n}^v$ and $\theta_{T,n}^v$, $\forall n \in \mathcal{N}$. Problem **(P4)-sdr** ends up to

$$\begin{aligned} \max_{\beta_{R,n}^v, \beta_{T,n}^v \in [0,1]} \quad & (\chi_{R,n}^v \beta_{R,n}^v + \chi_{T,n}^v \beta_{T,n}^v) \quad (75) \\ \text{s.t.} \quad & (\beta_{R,n}^v)^2 + (\beta_{T,n}^v)^2 = 1 \end{aligned}$$

where $\chi_{a,n}^v \triangleq \beta_{a,n}^{v*} \cos(\theta_{a,n}^{v*} - \theta_{a,n}^v)$, with $\beta_{a,n}^{v*} e^{j\theta_{a,n}^{v*}}$ obtained by solving **(P4)-sdr**, for $a \in \{T, R\}$ and $v \in \{p, c\}$. Such an amplitude-only subproblem is the maximization of a linear function over the unit circle, which admits the following closed-form solutions:

- If $\chi_{R,n}^v \geq 0$ and $\chi_{T,n}^v \geq 0$, then

$$\hat{\beta}_{a,n}^v = \frac{\chi_{a,n}^v}{\sqrt{(\chi_{R,n}^v)^2 + (\chi_{T,n}^v)^2}} \quad \text{for } a \in \{T, R\}.$$

- If $\chi_{R,n}^v \geq 0$ and $\chi_{T,n}^v < 0$, then

$$\hat{\beta}_{R,n}^v = 1 \quad \text{and} \quad \hat{\beta}_{T,n}^v = 0.$$

- If $\chi_{R,n}^v < 0$ and $\chi_{T,n}^v \geq 0$, then

$$\hat{\beta}_{R,n}^v = 0 \quad \text{and} \quad \hat{\beta}_{T,n}^v = 1.$$

- If $\chi_{R,n}^v < 0$ and $\chi_{T,n}^v < 0$, then

$$\left(\hat{\beta}_{R,n}^v, \hat{\beta}_{T,n}^v \right) = \begin{cases} (0, 1), & \chi_{T,n}^v \geq \chi_{R,n}^v \\ (1, 0), & \chi_{R,n}^v > \chi_{T,n}^v \end{cases}.$$

We note that, when both $\chi_{R,n}^v$ and $\chi_{T,n}^v$ are positive, the optimum lies in the interior of the first quadrant. Otherwise, the solution occurs at the boundary of the feasible set.

G. Overall alternating optimization procedure

The optimization problems addressed in Subsections III-C, III-D, III-E, and III-F provide update rules and tractable subroutines for each variable block. In this subsection we describe how these blocks are coordinated to solve the original problem **(P1)-mod**. We adopt a block coordinate descent (BCD) framework [66], where at each iteration one block of variables is updated while keeping the others fixed. More specifically, we resort to a penalty parameter updating strategy, widely used in augmented-Lagrangian and constrained non-convex optimization [67], [68], which enables the BCD algorithm to first locate a reliable operating point in a relaxed feasible region and subsequently enforce the physical STAR-RIS constraints. This continuation mechanism mitigates poor stationary points commonly encountered in tightly coupled non-convex beamforming problems.

During the preparation stage, the algorithm updates the variables sequentially as follows:

- 1) Update the variables $\bar{\tau}^p$ and $\bar{\rho}^p$ using (43) and (46).
- 2) Update the BS beamforming matrix \mathbf{W} by solving problem **(P2)** in (47a)–(47c) via SCA.
- 3) Update the STAR-RIS partition vector \mathbf{b} using the penalized relaxation and projection in Subsection III-D.
- 4) Update the STAR-RIS coefficients (Φ_T^p, Φ_R^p) by solving the SDR problem **(P4)-sdr** in (65a)–(65d) and applying rank-one recovery.
- 5) Recover feasible element coefficients via the element-wise projection in Subsection III-F.

During the communication stage, sensing constraints are inactive and all elements operate in ES mode ($\mathbf{b} = \mathbf{1}_N$). The updates reduce to the following steps:

- 1) Update $\bar{\tau}^c$ and $\bar{\rho}^c$ using (43) and (46).
- 2) Update \mathbf{W} by solving the convex communication-only beamforming problem [58], [61], [62].
- 3) Update (Φ_T^c, Φ_R^c) by solving the SDR problem **(P4)-sdr** in (65a)–(65d) and applying rank-one recovery.
- 4) Recover feasible element coefficients via the element-wise projection in Subsection III-F.

Each block update either (i) maximizes the objective with the remaining variables fixed, or (ii) maximizes a tight surrogate (SCA) that lower-bounds the original cost. Hence, the sequence of objective values is monotonically non-decreasing and upper bounded due to the finite transmit power. By standard results for block-coordinate methods (see, e.g., [66]–[68]), the procedure converges to a stationary point of the original problem under mild regularity conditions.

In practice we terminate the outer loop when the relative improvement of the objective between two successive outer iterations is below a threshold ϵ (e.g., 10^{-3}) or when a maximum number of iterations I_{\max} is reached. Inner subproblems (SDPs/SCA) are solved to moderate tolerances to balance accuracy and runtime. The computational bottleneck is represented by the SDP solvers in problem **(P4)-sdr** (Section III-E). Their complexity scales polynomially with the STAR-RIS dimension N (roughly cubic for interior-point solvers). The SCA and projection steps are comparatively inexpensive. For large-scale arrays, first-order SDP solvers or

Table I: Main characteristics of the considered benchmark schemes.

Scheme	Sensing SNR	Phase coupling	Spatial expectation statistics	Minimum rate guarantee	Manifold design	Dual stage
Proposed	Yes	Yes	Yes	No	Yes	Yes
CPS-STAR [31]	No	Yes	No	No	No	No
IPS-STAR [7], [32]	No	No	No	Yes	No	No
NoStat-STAR	Yes	Yes	No	No	Yes	Yes
Fixed-STAR	Yes	Yes	Yes	No	No	Yes

low-rank approximations can be employed. However, this is outside the current paper's scope and is left for future work.

IV. NUMERICAL RESULTS

This section evaluates the performance of the proposed STAR-RIS-assisted ISAC framework through Monte Carlo numerical simulations. The objective is to assess the achievable communication-sensing tradeoff and to quantify the benefits of jointly optimizing beamforming weights, metasurface coefficients, and element partitioning. To this end, the proposed design is compared with several benchmark schemes representing different modeling assumptions and levels of optimization capability. Specifically, the following benchmark schemes are considered for performance evaluation.

- 1) *Coupled phase-shift STAR-RIS (CPS-STAR)*: This scheme follows the coupled phase model introduced in [31], where the transmission and reflection coefficients satisfy a fixed phase-difference constraint. It serves as a reference implementation of STAR-RIS designs explicitly accounting for phase coupling.
- 2) *Phase-independent STAR-RIS (IPS-STAR)*: Based on [7], [32], this approach optimizes the communication sum-rate while ignoring the phase-coupling relation between transmission and reflection coefficients; it enforces a minimum user-rate constraint.
- 3) *Proposed STAR-RIS without statistical information (NoStat-STAR)*: This scheme relies on the proposed optimization framework but neglects the spatial statistical information used in the main design. It is introduced to isolate the performance gain obtained from exploiting error estimation statistics.
- 4) *Proposed STAR-RIS with fixed manifold (Fixed-STAR)*: Here, the metasurface configuration is predetermined and not optimized. Specifically, half of the elements operate in transmission-only mode, while the remaining elements operate in reflection-only mode. This scheme evaluates the benefit of adaptive element partitioning.

The main characteristics of the considered benchmark schemes are summarized in Table I.

According to Fig. 3, the STAR-RIS is placed at the origin $(0, 0, 0)$ m, while the BS is located at $(20, 30, 0)$ m. The number of users in the transmission and reflection regions are assumed to be equal, i.e., $K_T = K_R$. The random position of user k can be expressed in spherical coordinates as

$$\mathbf{p}_k = \begin{cases} (r_k, \phi_k, \varphi_k), & k \in \mathcal{K}_T \\ (r_k, \phi_k + \Delta\phi_k, \varphi_k + \Delta\varphi_k), & k \in \mathcal{K}_R \end{cases} \quad (76)$$

Table II: Simulation setting.

Parameter	Value
Number of antennas at the BS	$M = 8$
Number of sensors	$N_s = 8$
Number of users	$K = 4$
Number of STAR-RIS elements	$N = 20$
Transmit power of BS	$\mathcal{P}_{\max} = 20$ dBm
Rician factor	$\mu_1 = \mu_{2,\text{in}} = \mu_{2,\text{out}} = 2$
Noise power	$\sigma_{n_u}^2 = \sigma_{n_s}^2 = -110$ dBm
Path loss at $d_0 = 1$ m	$\zeta_0 = 30$ dB
Sensing SNR threshold	$\delta_{\text{sens}} = 10$ dB
Number of ES elements	$N_{\text{part}} = 10$
Sensing complex amplitude	$\alpha_k = -10$ dB

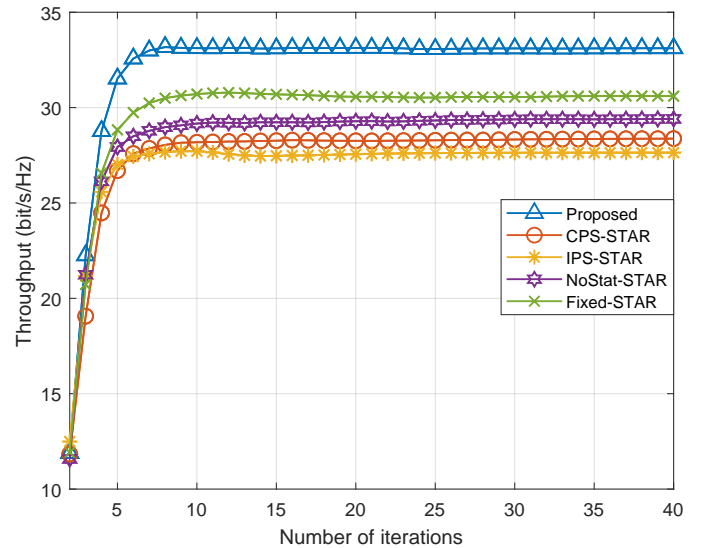


Figure 4: Throughput versus number of iterations.

with $r_k \sim \mathcal{U}[30, 50]$ m, $\phi_k \sim \mathcal{U}[0^\circ, 180^\circ]$, and $\varphi_k \sim \mathcal{U}[-90^\circ, 90^\circ]$, where the angular uncertainties are modeled as $\Delta\phi_k, \Delta\varphi_k \sim \mathcal{N}(0, \text{PCRB})$, with the PCRB given in [31]. The remaining system parameters are summarized in Table II. This baseline configuration is kept unchanged across all simulation results unless otherwise specified.

A. Throughput as a function of the number of iterations

The convergence behavior of the proposed algorithm is evaluated in terms of the achievable throughput, whose evolution over the iterations is illustrated in Fig. 4. The curve exhibits monotonic convergence within a limited number (about 10) of iterations. In addition, results not reported here show that the phase difference stabilizes around $\pi/2$ and $3\pi/2$ after approximately 15 iterations. As can be observed from Fig. 4,

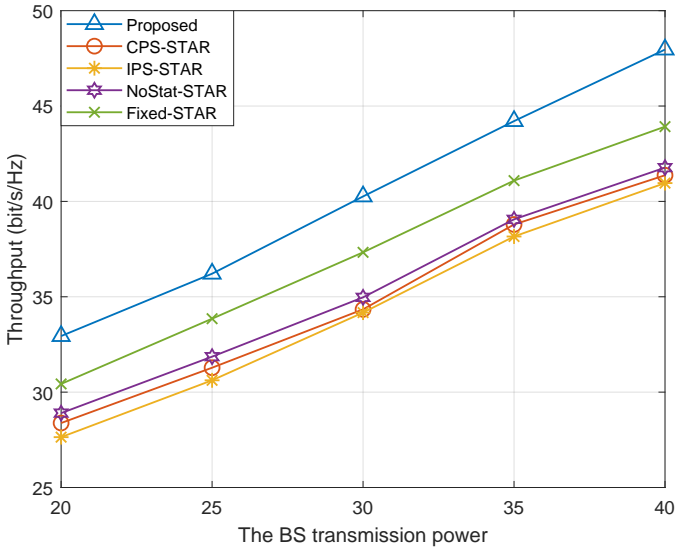


Figure 5: Throughput versus BS power.

CPS-STAR, IPS-STAR, and NoStat-STAR methods provide comparable performances, since none of them explicitly takes into account spatial-domain constraints. Among them, NoStat-STAR scheme achieves about a 4% performance improvement over the CPS-STAR and IPS-STAR approaches. This difference originates from the distinct optimization constraints adopted by the considered designs, which lead to different operating tradeoffs while still confirming the feasibility of the proposed framework. The performance gap becomes more evident when compared with the Fixed-STAR scheme. Its fixed architecture limits design flexibility and inherently constrains the achievable performance. Moreover, the restricted effective aperture deteriorates unbiased estimation accuracy, which may further amplify beam misalignment under non-ideal conditions. Overall, the results show that incorporating spatial-domain requirements yields a 13.98% performance gain for the proposed scheme, while the increased design flexibility provides an additional 8.24% improvement.

B. Throughput as a function of the BS power budget

The variation of the achievable throughput w.r.t. the BS transmit power is shown in Fig. 5. As expected, the achievable rate increases with the transmit power, since higher available power results in greater signal strength at the users. It can be observed that IPS-STAR, NoStat-STAR, and Fixed-STAR schemes exhibit similar performance levels, whereas the proposed method consistently achieves about 14% higher rate values.

C. Throughput as a function of the number of STAR-RIS elements

The achievable throughput as a function of the number N of STAR-RIS elements is shown in Fig. 6. For all considered schemes, the achievable rate increases as the number of metasurface elements grows. The proposed method exhibits an improvement of approximately 14% for each doubling of the element count. This behavior is expected, since a larger

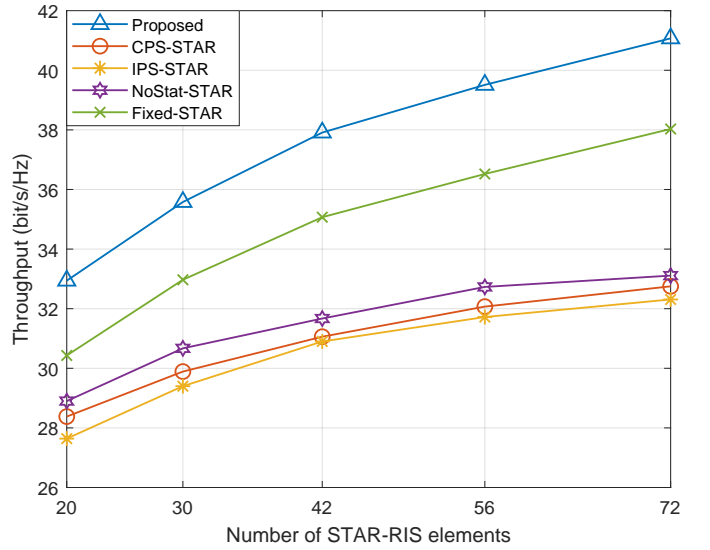


Figure 6: Throughput versus metasurface number of elements.

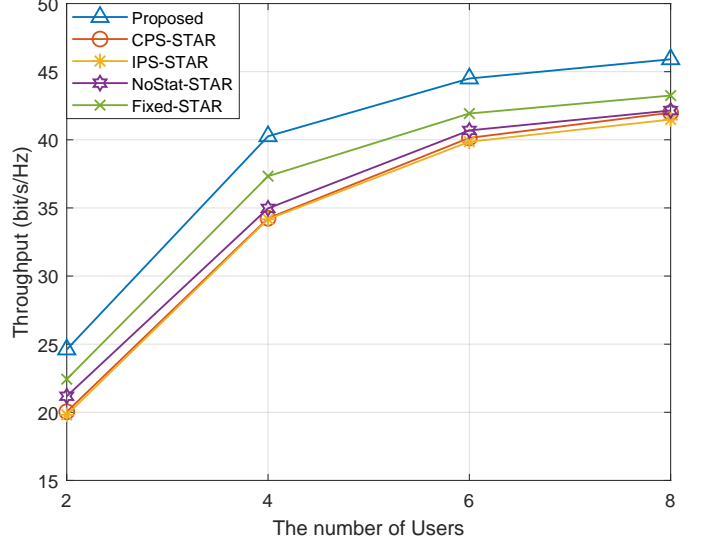


Figure 7: Throughput versus number of users.

STAR-RIS provides higher values of the beamforming gain. Furthermore, the increased aperture enhances angle estimation accuracy, resulting in improved beam alignment. The additional design flexibility offered by the proposed scheme further contributes to its performance advantage.

D. Throughput as a function of the number of users

The achievable throughput as a function of the number of users is shown in Fig. 7. The results are obtained under the condition $K_T = K_R$ and in the presence of angle estimation errors in the reflection space. All schemes exhibit sublinear growth as the number of users increases, due to intensified resource competition and the resulting inter-user interference. The absence of a minimum per-user rate constraint in the formulation further accentuates this behavior. The proposed method maintains a rate gain of approximately 12% – 15% for $K \leq 6$, which gradually decreases to about 8% at $K = 8$.

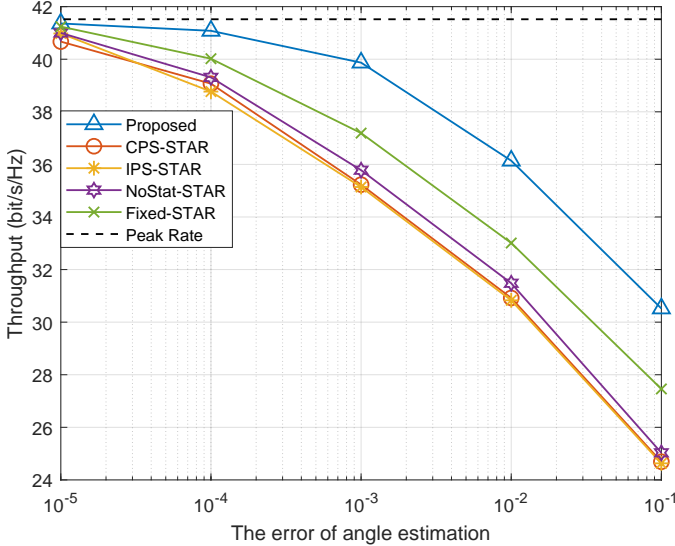


Figure 8: Throughput versus DOA estimation error.

E. Throughput as a function of angle estimation error

The achievable throughput as a function of the estimation error is shown in Fig. 8. Here, the peak throughput corresponds to the achievable rate under perfect angular knowledge. As the estimation error decreases, all schemes under comparison gradually approach the performance of the ideal error-free case. At $\Delta\phi_k = \Delta\varphi_k = 0.1^\circ$, the proposed method experiences a noticeable performance degradation; nevertheless, it still outperforms the other algorithms by approximately 25%. For $\Delta\phi_k = \Delta\varphi_k = 0.001^\circ$, the proposed scheme exhibits strong robustness, showing only an 8% performance loss relative to the ideal case. This operating point is already close to the practical resolution limits of typical DOA estimation systems. When the angular estimation error further decreases to $\Delta\phi_k = \Delta\varphi_k = 0.0001^\circ$, all methods asymptotically converge to the unbiased optimization baseline. Despite this convergence, the proposed scheme maintains a residual performance advantage of about 4%, which can be attributed to its increased architectural flexibility.

V. CONCLUSIONS

This paper investigated the design of a STAR-RIS-assisted ISAC systems from a protocol-level perspective. By leveraging the full-space transmission and reflection capabilities of STAR-RISs, a two-stage ISAC protocol was proposed, in which a preparation phase supports direction estimation and communication, while a subsequent communication phase exploits the acquired angular information to enhance information transfer. Differently from most existing works, the system design explicitly takes into account the distinct roles of the two stages and jointly optimizes the corresponding transmission strategies.

To capture the impact of sensing uncertainty on communication performance, the directions of outdoor users were modeled as random variables, and the average achievable rate was incorporated into the system design. A performance-balanced optimization problem was formulated, jointly optimizing the

BS beamforming weights, the STAR-RIS transmission and reflection coefficients in both stages, and the metasurface partition between ES and TO modes, while explicitly enforcing STAR-RIS physical feasibility constraints and sensing-quality requirements. To tackle the resulting non-convex and mixed discrete-continuous problem, an efficient solution framework based on fractional programming, Lagrangian dual reformulation, successive convex approximation, and semidefinite relaxation was developed.

Simulation results have demonstrated that the proposed design achieves a favorable trade-off between sensing accuracy and communication throughput, exhibiting a remarkable robustness against DOA estimation errors. Compared with conventional STAR-RIS-aided ISAC schemes that neglect protocol-level optimization or sensing uncertainties, the proposed framework provides consistent performance gains under both ideal and imperfect sensing conditions.

Future deployments could exploit the low-power, facade-mounted STAR-RIS ISAC architecture to deliver scalable, spectrum-efficient IoT connectivity across urban infrastructures, bridging communication and localization needs for emerging smart-city services.

REFERENCES

- [1] C. L. Holloway, E. F. Kuester, J. A. Gordon, J. O'Hara, J. Booth, and D. R. Smith, "An overview of the theory and applications of metasurfaces: The two-dimensional equivalents of metamaterials," *IEEE Antennas Propag. Mag.*, vol. 54, no. 2, pp. 10–35, Apr. 2012.
- [2] M. Di Renzo *et al.*, "Smart radio environments empowered by reconfigurable intelligent surfaces: How it works, state of research, and the road ahead," *IEEE J. Sel. Areas Commun.*, vol. 38, no. 11, pp. 2450–2525, Nov. 2020.
- [3] D. Kudathanthirige, D. Gunasinghe, and G. Amarasuriya, "Performance analysis of intelligent reflective surfaces for wireless communication," in *Proc. IEEE Int. Conf. Commun. (ICC)*, Dublin, Ireland, Jun. 2020, pp. 1–6.
- [4] W. Tang *et al.*, "Wireless communications with reconfigurable intelligent surface: Path loss modeling and experimental measurement," *IEEE Trans. Wireless Commun.*, vol. 20, no. 1, pp. 421–439, Jan. 2021.
- [5] T. J. Cui, M. Q. Qi, X. Wan, J. Zhao, and Q. Cheng, "Coding metamaterials, digital metamaterials and programmable metamaterials," *Light Sci. Appl.*, vol. 3, Art. no. e218, Oct. 2014.
- [6] C. Huang, B. Sun, W. Pan, J. Cui, X. Wu, and X. Luo, "Dynamical beam manipulation based on 2-bit digitally-controlled coding metasurface," *Sci. Rep.*, vol. 7, Art. no. 42302, Feb. 2017.
- [7] Z. Liu, X. Li, H. Ji, H. Zhang, and V. C. M. Leung, "Toward STAR-RIS-empowered integrated sensing and communications: Joint active and passive beamforming design," *IEEE Trans. Veh. Technol.*, vol. 72, no. 12, pp. 15991–16005, Dec. 2023.
- [8] K. Meng, Q. Wu, W. Chen, and D. Li, "Sensing-assisted communication in vehicular networks with intelligent surface," *IEEE Trans. Veh. Technol.*, vol. 73, no. 1, pp. 876–893, Jan. 2024.
- [9] M. Li, S. Zhang, Y. Ge, Z. Li, F. Gao, and P. Fan, "STAR-RIS-aided integrated sensing and communication over high-mobility scenario," *IEEE Trans. Commun.*, vol. 72, no. 8, pp. 4788–4802, Aug. 2024.
- [10] Q. Wang *et al.*, "STAR-RIS-aided covert communication in UAV air-ground networks," *IEEE J. Sel. Areas Commun.*, vol. 43, no. 1, pp. 245–259, Jan. 2025.
- [11] Z. Yigit and E. Basar, "Hybrid STAR-RIS enabled integrated sensing and communication," *IEEE Trans. Commun.*, vol. 73, no. 9, pp. 8289–8300, Sep. 2025.
- [12] L. Bao, Q. Ma, R. Y. Wu, X. Fu, J. Wu, and T. J. Cui, "Programmable reflection-transmission shared-aperture metasurface for real-time control of electromagnetic waves in full space," *Adv. Sci.*, vol. 8, no. 15, Art. no. 2100149, Aug. 2021.
- [13] X. Mu, Y. Liu, L. Guo, J. Lin, and R. Schober, "Simultaneously transmitting and reflecting (STAR) RIS aided wireless communications," *IEEE Trans. Wireless Commun.*, vol. 21, no. 5, pp. 3083–3098, May 2022.

[14] J. Xu, Y. Liu, X. Mu, and O. A. Dobre, "STAR-RISs: Simultaneous transmitting and reflecting reconfigurable intelligent surfaces," *IEEE Commun. Lett.*, vol. 25, no. 9, pp. 3134–3138, Sep. 2021.

[15] H. Zhang *et al.*, "Intelligent omni-surfaces for full-dimensional wireless communications: Principles, technology, and implementation," *IEEE Commun. Mag.*, vol. 60, no. 2, pp. 39–45, Feb. 2022.

[16] Q. Hu *et al.*, "An intelligent programmable omni-metasurface," *Laser Photon. Rev.*, vol. 16, no. 6, Art. no. 2100718, Jun. 2022.

[17] F. Verde, V. Galdi, L. Zhang, and T. J. Cui, "Integrating sensing and communications: Simultaneously transmitting and reflecting digital coding metasurfaces: A successful convergence of physics and signal processing," *IEEE Signal Process. Mag.*, vol. 41, no. 5, pp. 56–70, Sep. 2024.

[18] Y. Liu, X. Mu, J. Xu, R. Schober, Y. Hao, H. V. Poor, and L. Hanzo, "STAR: Simultaneous transmission and reflection for 360° coverage by intelligent surfaces," *IEEE Wireless Commun.*, vol. 28, no. 6, pp. 102–109, Dec. 2021.

[19] R. Zhong, Y. Liu, X. Mu, Y. Chen, X. Wang, and L. Hanzo, "Hybrid reinforcement learning for STAR-RISs: A coupled phase-shift model based beamformer," *IEEE J. Sel. Areas Commun.*, vol. 40, no. 9, pp. 2556–2569, Sep. 2022.

[20] J. Xu, Y. Liu, X. Mu, R. Schober, and H. V. Poor, "STAR-RISs: A correlated TR phase-shift model and practical phase-shift configuration strategies," *IEEE J. Sel. Topics Signal Process.*, vol. 16, no. 5, pp. 1097–1111, Aug. 2022.

[21] H. Zhu, Y. Liu, Y.-C. Wu, and V. K. N. Lau, "A unified framework for STAR-RIS coefficients optimization," *IEEE Trans. Signal Process.*, vol. 72, pp. 5107–5122, July 2024.

[22] Y. Liu, X. Mu, R. Schober, and H. V. Poor, "Simultaneously transmitting and reflecting (STAR)-RISs: A coupled phase-shift model," in *Proc. IEEE Int. Conf. Commun. (ICC)*, Seoul, South Korea, May 2022, pp. 2840–2845.

[23] S. Huang, W. Wang, S. Ren, and H. Dang, "Min-max fairness-based beamforming design for coupled phase shift STAR-RIS-assisted MIMO system," *IEEE Internet Things J.*, vol. 12, no. 3, pp. 3145–3162, Feb. 2025.

[24] Z. Wang, X. Mu, Y. Liu, and R. Schober, "Coupled phase-shift STAR-RISs: A general optimization framework," *IEEE Wireless Commun. Lett.*, vol. 12, no. 2, pp. 207–211, Feb. 2023.

[25] Y. Wu, C. Zhang, H. Hai, and E. Bai, "Average sum-rate maximization of coupled phase-shift STAR-RIS-assisted SWIPT-NOMA system," *IEEE Commun. Lett.*, vol. 28, no. 12, pp. 2889–2893, Dec. 2024.

[26] X. Ju, S. Gong, N. Zhao, C. Xing, A. Nallanathan, and D. Niyato, "A framework on complex matrix derivatives with special structure constraints for wireless systems," *IEEE Trans. Commun.*, vol. 72, no. 8, pp. 5145–5161, Aug. 2024.

[27] T. Cai *et al.*, "High-efficiency and full-space manipulation of electromagnetic wave fronts with metasurfaces," *Phys. Rev. Appl.*, vol. 8, no. 3, Art. no. 034033, Sep. 2017.

[28] X. Wang, J. Ding, B. Zheng, S. An, G. Zhai, and H. Zhang, "Simultaneous realization of anomalous reflection and transmission at two frequencies using bifunctional metasurfaces," *Sci. Rep.*, vol. 8, no. 1, Art. no. 1876, Jan. 2018.

[29] Y. Cui, F. Liu, X. Jing, and J. Mu, "Integrating sensing and communications for ubiquitous IoT: Applications, trends, and challenges," *IEEE Netw.*, vol. 35, no. 5, pp. 158–167, Sep./Oct. 2021.

[30] F. Dong *et al.*, "Communication-assisted sensing in 6G networks," *IEEE J. Select. Areas Commun.*, vol. 43, no. 4, pp. 1371–1386, Apr. 2025.

[31] Z. Wang, X. Mu, and Y. Liu, "STARs enabled integrated sensing and communications," *IEEE Trans. Wireless Commun.*, vol. 22, no. 10, pp. 6750–6765, Oct. 2023.

[32] S. Zhang *et al.*, "Joint beamforming optimization for active STAR-RIS-assisted ISAC systems," *IEEE Trans. Wireless Commun.*, vol. 23, no. 11, pp. 15888–15902, Nov. 2024.

[33] S. Zhang, W. Hao, G. Sun, Z. Zhu, X. Li, and Q. Wu, "Joint beamforming design for the STAR-RIS-enabled ISAC systems with multiple targets and multiple users," *IEEE Trans. Commun.*, vol. 73, no. 1, pp. 693–708, Jan. 2025.

[34] T. Zhou *et al.*, "STAR-RIS-empowered integrated sensing and covert communication system with movable elements: Joint robust beamforming and element deployment design," *IEEE Trans. Cogn. Commun. Netw.*, vol. 11, no. 5, pp. 2893–2909, Oct. 2025.

[35] Q. Li, K. Huang, X. Wang, K. Liu, and M. Yi, "Simultaneously transmitting and reflecting reconfigurable intelligent surface assisted full space direction-of-arrival estimation," in *Proc. Int. Conf. Microw. Millim. Wave Technol. (ICMWT)*, Beijing, China, 2024, pp. 1–3.

[36] L. Li, L. He, Y. Li, and P. S. R. Diniz, "Robust RIS-based DOA estimation with mixed constraints," *IEEE Signal Process. Lett.*, vol. 31, pp. 2260–2264, 2024.

[37] Y. Tian, Y. Feng, W. Liu, H. Chen, and G. Wang, "Reconfigurable intelligent surface aided DOA estimation by a single receiving antenna," *IEEE Trans. Commun.*, vol. 73, no. 2, pp. 983–994, Feb. 2025.

[38] H. Chung and S. Kim, "Location-aware beam training and multi-dimensional ANM-based channel estimation for RIS-aided mmWave systems," *IEEE Trans. Wireless Commun.*, vol. 23, no. 1, pp. 652–666, Jan. 2024.

[39] Y. Mehmood, F. Ahmad, I. Yaqoob, A. Adnane, M. Imran, and S. Guizani, "Internet-of-things-based smart cities: Recent advances and challenges," *IEEE Commun. Mag.*, vol. 55, no. 9, pp. 16–24, Sep. 2017.

[40] M. Ahmed *et al.*, "A survey on STAR-RIS: Use cases, recent advances, and future research challenges," *IEEE Internet Things J.*, vol. 10, no. 16, pp. 14689–14711, Aug. 2023.

[41] D. Darsena, G. Gelli, I. Iudice and F. Verde, "Sensing technologies for crowd management, adaptation, and information dissemination in public transportation systems: A review," *IEEE Sens. J.*, vol. 23, no. 1, pp. 68–87, Jan. 2023.

[42] 3GPP, "Study on channel model for frequencies from 0.5 to 100 GHz," 3GPP TR 38.901, Ver. 17.0.0, Dec. 2022.

[43] ITU-R, "Prediction of building entry loss," Recommendation ITU-R P.2109-2, 2023.

[44] T. S. Rappaport *et al.*, *Millimeter Wave Wireless Communications*. Pearson, 2015.

[45] F. Zafari, A. Gkelias, and K.K. Leung, "A survey of indoor localization systems and technologies," *IEEE Commun. Surv. Tutor.*, vol. 21, no. 3, pp. 2568–2599, thirdquarter 2019.

[46] Z. Liu, T. Chen, M. Guo, and F. Verde "STAR-RIS-assisted full-space angle estimation via finite rate of innovation", arXiv:2602.02893, Feb. 2026.

[47] J. Shabaniour and C. R. Simovski, "Angular and polarization stability of broadband reconfigurable intelligent surfaces of binary type," *IEEE Access*, vol. 10, pp. 126253–126268, 2022.

[48] B. O. Zhu *et al.*, "Dynamic control of electromagnetic wave propagation with the equivalent principle inspired tunable metasurface," *Sci. Rep.*, vol. 4, Art. no. 4971, 2014.

[49] C. Sturm and W. Wiesbeck, "Waveform design and signal processing aspects for fusion of wireless communications and radar sensing," *Proc. IEEE*, vol. 99, no. 7, pp. 1236–1259, July 2011.

[50] F. Liu, Y.-F. Liu, A. Li, C. Masouros, and Y.C. Eldar, "Cramér–Rao bound optimization for joint radar-communication beamforming," *IEEE Trans. Signal Process.*, vol. 68, pp. 2401–2415, 2022.

[51] W. Yuan, F. Liu, C. Masouros, J. Yuan, D. W. K. Ng, and N. González-Prelcic, "Bayesian predictive beamforming for vehicular networks: A low-overhead joint radar-communication approach," *IEEE Trans. Wireless Commun.*, vol. 20, no. 3, pp. 1442–1456, Mar. 2021.

[52] S. M. Kay, *Fundamentals of Statistical Signal Processing: Estimation Theory*. Englewood Cliffs, NJ, USA: Prentice-Hall, 1993.

[53] P. Stoica and A. Nehorai, "MUSIC, maximum likelihood, and Cramér–Rao bound," *IEEE Trans. Acoust., Speech, Signal Process.*, vol. 37, no. 5, pp. 720–741, May 1989.

[54] R. Roy and T. Kailath, "ESPRIT—estimation of signal parameters via rotational invariance techniques," *IEEE Trans. Acoust., Speech, Signal Process.*, vol. 37, no. 7, pp. 984–995, Jul. 1989.

[55] X. Shao, C. You, W. Ma, X. Chen, and R. Zhang, "Target sensing with intelligent reflecting surface: Architecture and performance," *IEEE J. Sel. Areas Commun.*, vol. 40, no. 7, pp. 2070–2084, Jul. 2022.

[56] H. L. Van Trees, *Optimum Array Processing: Part IV of Detection, Estimation, and Modulation Theory*. Hoboken, NJ, USA: Wiley, 2004.

[57] H. Krim and M. Viberg, "Two decades of array signal processing research: The parametric approach," *IEEE Signal Process. Mag.*, vol. 13, no. 4, pp. 67–94, Jul. 1996.

[58] S. Boyd and L. Vandenberghe, *Convex Optimization*. Cambridge, U.K.: Cambridge Univ. Press, 2004.

[59] K. Shen and W. Yu, "Fractional programming for communication systems—Part I: Power control and beamforming," *IEEE Trans. Signal Process.*, vol. 66, no. 10, pp. 2616–2630, May 2018.

[60] K. Shen and W. Yu, "Fractional programming for communication systems—Part II: Uplink scheduling via matching," *IEEE Trans. Signal Process.*, vol. 66, no. 10, pp. 2631–2644, May 2018.

[61] D. Tse and P. Viswanath, *Fundamentals of Wireless Communication*. Cambridge, U.K.: Cambridge Univ. Press, 2005.

[62] A. Beck, *Introduction to Nonlinear Optimization: Theory, Algorithms, and Applications with Python and MATLAB*. MOS-SIAM Series on Optimization, 2014.

- [63] D. P. Palomar, *Portfolio Optimization: Theory and Application*. Cambridge, U.K.: Cambridge Univ. Press, 2025.
- [64] R. A. Horn and C. R. Johnson, *Matrix Analysis*. Cambridge, U.K.: Cambridge Univ. Press, 1990.
- [65] D.H. Brandwood, “A complex gradient operator and its application in adaptive array theory,” *IEE Proceedings F - Communications, Radar and Signal Processing*, vol. 130, no. 1, pp. 11–16, Feb. 1983.
- [66] D. P. Bertsekas, *Nonlinear Programming*, 2nd ed. Belmont, MA, USA: Athena Scientific, 1999.
- [67] D. P. Bertsekas, *Constrained Optimization and Lagrange Multiplier Methods*. Belmont, MA, USA: Athena Scientific, 1996.
- [68] M. Razaviyayn, M. Hong, and Z.-Q. Luo, “A unified convergence analysis of block successive minimization methods for nonsmooth optimization,” *SIAM Journal on Optimization*, vol. 23, no. 2, pp. 1126–1153, 2013.